



Published in final edited form as:

Nat Cell Biol. 2018 May ; 20(5): 586–596. doi:10.1038/s41556-018-0084-5.

Loss of KLHL6 promotes diffuse large B-cell lymphoma growth and survival by stabilizing the mRNA decay factor Roquin2

Jaewoo Choi¹, Kyutae Lee¹, Kristin Ingvarsdottir², Roberto Bonasio², Anita Saraf³, Laurence Florens³, Michael P. Washburn^{3,4}, Saber Tadros⁵, Michael R. Green^{5,6}, and Luca Busino¹

¹Department of Cancer Biology, University of Pennsylvania, Philadelphia, PA 19104; Perelman School of Medicine and Abramson Family Cancer Research Institute, University of Pennsylvania, Philadelphia, PA 19104, USA

²Epigenetics Institute; Department of Cell and Developmental Biology, University of Pennsylvania, Philadelphia, PA 19104, USA

³The Stowers Institute of Medical Research, 1000 East 50th Street, Kansas City, MO 64110, USA

⁴Department of Pathology and Laboratory Medicine, The University of Kansas Medical Center, Kansas City, KS 66150, USA

⁵Department of Lymphoma/Myeloma, University of Texas MD Anderson Cancer Center, Houston, TX 77030, USA

⁶Department of Genomic Medicine, University of Texas MD Anderson Cancer Center, Houston, TX 77030, USA

Abstract

Kelch-like protein 6 (KLHL6) is an uncharacterized gene mutated in diffuse large B-cell lymphoma (DLBCL). We report that KLHL6 assembles with CULLIN3 to form a functional CULLIN-Ring ubiquitin ligase. Mutations of KLHL6 inhibit its ligase activity by disrupting the interaction with CULLIN3. Loss of KLHL6 favors DLBCL growth and survival both *in vitro* and in xenograft models. We further established the mRNA decay factor Roquin2 as a substrate of KLHL6. Degradation of Roquin2 is dependent on B-cell receptor activation, and requires the integrity of the tyrosine 691 in Roquin2 that is essential for its interaction with KLHL6. A non-degradable Roquin2 (Y691F) mutant requires its RNA binding ability to phenocopy the effect of KLHL6 loss. Stabilization of Roquin2 promotes mRNA decay of the tumor suppressor and NF- κ B

Users may view, print, copy, and download text and data-mine the content in such documents, for the purposes of academic research, subject always to the full Conditions of use: http://www.nature.com/authors/editorial_policies/license.html#terms

Correspondence and requests for materials should be addressed to L.B. (businol@upenn.edu).

Author Contributions. L.B. conceived, directed the project and oversaw the results. J.C. designed and performed most experiments. K.L. helped J.C. with experiments in Fig. 1i, 3b, 3d, 4h, 6a, 7h, 7j, S3b, and S4h. K.I. helped J.C. with experiments in Fig. 6b. R.B. helped with the bioinformatics analysis of RNA-seq data. A.S., L.F. and M.P.W. performed the mass spectrometry analysis of the KLHL6 complex purified by L.B.. M.G. and S.T. helped with Fig. 1a, 1b and 3a, 7g, S1a, S1b, S7e, and S7f. L.B. and J.C. wrote the manuscript.

Author Information. The authors declare no competing financial interests.

pathway inhibitor, tumor necrosis factor- α -inducible gene 3 (TNFAIP3). Collectively, our findings uncover the tumor suppressing mechanism of KLHL6.

Introduction

B-cell cancers hijack protein ubiquitylation and degradation to promote growth and survival, as shown by the successful use of a proteasome inhibitor (bortezomib) and E3 ubiquitin ligase inhibitor (lenalinomide) in multiple myeloma (MM) and mantle cell lymphoma¹. Despite the significant progress, much remains to be explored in the field of ubiquitin and molecular mechanisms of tumorigenesis.

Kelch-like protein 6 (KLHL6) is a member of the bric-a-brac/tramtrack/broad-complex (BTB) domain family of proteins with a lymphoid tissue-restricted expression pattern^{2,3}. Whole-genome and exome sequencing have revealed cancer-associated mutations of the *KLHL6* gene in B-cell malignancies, including diffuse large B-cell lymphoma (DLBCL)⁴⁻⁷; however, the relevance of these mutations as well as the molecular function of KLHL6 is currently unknown.

DLBCL is the most common type of lymphoid malignancies with two distinct molecular subtypes: activated B cell-like (ABC) and germinal center B cell-like (GCB) lymphoma^{8,9}. ABC-DLBCLs depend on hyper-activation of the inhibitor of $\text{I}\kappa\text{B}$ kinase (IKK) and the NF- κB transcription factor program for their proliferation and survival^{10,11}. This is evidenced by frequent mutations in the BCR pathway, including activating mutations of positive (*CD79A/B* and *CARD11*^{12,13}) and inactivating mutations of negative (*TNFAIP3*¹²⁻¹⁵) NF- κB regulators. How *KLHL6* contributes to the pathology of human DLBCL and whether it influences NF- κB activation are currently unknown.

Regulatory networks that promote cancer progression modulate gene expression at the level of mRNA stability^{16,17}. The RNA-binding proteins RC3H1 and RC3H2 (from now on Roquin1 and Roquin2) promote mRNA decay via recognition of stem-loop motifs in the 3' untranslated region (UTR) of target mRNAs^{18,19}. Through this recognition, Roquins recruit the CCR4-CAF1-NOT complex, leading to mRNA deadenylation and subsequent destabilization¹⁸⁻²². In T-cells, Roquin proteins contribute to immune homeostasis by promoting decay of Inducible T-cell Costimulator (ICOS). However, the role of Roquin in B-cell cancers has not been investigated^{18,23}.

Here, we demonstrate that KLHL6 is an E3 ligase for Roquin2. Cancer-associated mutations of KLHL6 inhibit its ubiquitin ligase activity and inactivation or loss of KLHL6 in ABC-DLBCL promotes cancer cell growth and survival through stabilization of Roquin2 and subsequent decay of the *TNFAIP3* mRNA. This study shows how ABC-DLBCL cells hijack the ubiquitin pathway to promote their proliferation via alteration of the mRNA decay process.

Results

KLHL6 mutations in human DLBCL abolish its catalytic function as cullin3-RING-ligase complex (CRL3)

Analysis of genomic databases of human mature B-cell cancer patients revealed mutations of the *KLHL6* gene in DLBCL (<http://cancergenome.nih.gov/> and^{4,5,6,7}), chronic lymphocytic leukemia (CLL)²⁴ and multiple myeloma (MM)²⁵ (Fig. 1a). DLBCL cohorts displayed the highest rate of genetic mutations (Fig. 1a), which are similarly stratified amongst GCB-DLBCL, ABC-DLBCL and uncharacterized DLBCL (Fig. 1b). Most mutations in DLBCL are missense and monoallelic, with a low number in non-sense and frameshift mutations (Fig. 1c, Supplementary Table 1 and^{4,5,6,7}). Majority of mutations clusters near and inside the BTB-domain of KLHL6 with mutational hotspots in Leucines 65 and 90 (Fig. 1c). Moreover, re-analysis of published SNP array data²⁶ revealed infrequent deletion of the *KLHL6* locus (Fig. S1a), while ~6% of DLBCL tumors displayed lower expression of *KLHL6* transcript (Fig. S1b).

To understand the impact of these cancer-associated mutations, we compared the protein interactome of KLHL6(WT) to that of the cancer mutant KLHL6(L65P). FLAG-KLHL6(WT) or FLAG-KLHL6(L65P) complexes were immunopurified from two cell lines (HEK293T and ARP-1) and the tryptic digestion of each protein eluate was analyzed by mass spectrometry (Supplementary Table 2). Unique spectral counts corresponding to CULLIN3 were identified in KLHL6(WT), but not in KLHL6(L65P) immunoprecipitates (Fig. 1d and Supplementary Table 2).

We validated our proteomic analysis via immunoprecipitation of KLHL6 with endogenous CULLIN3, but not CULLIN1, in HEK293T cells (Fig. 1e). By carrying out an *in vitro* ubiquitylation assay, we found that KLHL6 promoted self-ubiquitylation and, notably, its BTB-domain alone [KLHL6(Kelch)] was sufficient in catalyzing self-polyubiquitylation to a greater degree (Fig. 1f). These data suggest that KLHL6 assembles a functional CULLIN3-RING ubiquitin Ligase (CRL3)²⁷ (Fig. 1j).

We then investigated the effect of DLBCL-associated BTB-domain mutations on KLHL6 ligase assembly and activity. All mutations tested (L65P, S94I, F97L) disrupted binding to CULLIN3 (Fig. 1g) and consequently led to a loss of self-polyubiquitylation *in vitro* (Fig. 1h). Correspondingly, the protein levels of BTB-domain KLHL6 mutants were remarkably high at steady state and displayed extended half-lives as compared to those of wild-type (Fig. 1i), suggesting loss of KLHL6 self-ubiquitylation affects its turnover in cells.

KLHL6 interacts with and promotes the ubiquitylation and degradation of Roquin2

Since KLHL6(L65P) is unable to promote ubiquitylation, we reasoned that it might trap (*i.e.* interact with, but not ubiquitylate) substrates (Fig. 1j). By ranking proteins by the number of unique spectral counts, we identified Roquin2 as a potential substrate (Fig. 2a and Supplementary Table 2).

In agreement with our proteomic data, KLHL6 specifically co-immunoprecipitated endogenous Roquin2 in HEK293T cells (Fig. 2b). The reciprocal co-immunoprecipitation

experiments confirmed Roquin2, but not Roquin1, as a KLHL6 interactor (Fig. 2c). This complex was also detectable at an endogenous level in DLBCL cells (Fig. S2a). Importantly, interaction between KLHL6 and Roquin2 required the intact Kelch domain in KLHL6 (Fig. S2b), further supporting substrate-like interaction²⁸.

In DLBCL cell lines, abundance of KLHL6 and Roquin2 displayed an inverse correlation (Fig. 2d and S2c). To investigate whether KLHL6 controls Roquin2 protein levels, we assessed Roquin2 protein turnover upon knockdown or knockout of KLHL6 in OCI-LY10 and U2932 cells, respectively. In both cases, down-regulation of KLHL6 significantly extended the half-life of Roquin2, but not that of Roquin1 (Fig. 2e, 2f and S2d).

Gain-of-function experiments showed that re-expression of KLHL6 in cell lines with low *KLHL6* expression (*i.e.*; HEK293T and HBL1, see Fig. 5a right panel) down-regulated Roquin2 protein levels (Fig. S2e). Moreover, BTB-domain mutants were incapable of inducing Roquin2 down-regulation (Fig. S2f). Notably, co-expression of KLHL6(WT) along with BTB-mutants still promoted Roquin2 degradation, suggesting these mutations are not dominant negative (Fig. S2g).

Next, we utilized B-cell lymphoma cell lines harboring endogenous *KLHL6* mutations. VAL cells harbor two BTB-mutations: N60T and T72R (Fig. 2g). Binding analysis revealed that only the KLHL6(T72R) mutant lost interaction with CULLIN3 (Fig. 2g), while KLHL6(N60T) mutant did not. Knockdown of KLHL6 in VAL cells did not result in Roquin2 accumulation (Fig. 2h), whereas re-expression of KLHL6 induced Roquin2 downregulation (Fig. 2j). In VAL cells, expression of *KLHL6* at the mRNA level was comparatively low (Fig. 2i). This suggests that VAL cells display one *KLHL6* allele inactivated by a mutation in the BTB-domain and an additional down-regulation of *KLHL6* mRNA. In contrast, mutations of *KLHL6* in SUDHL10 cells had no impact on KLHL6 function (Fig. 2g, 2h 2i, and 2j).

Lastly, to explore whether KLHL6 directly controls Roquin2 ubiquitylation *in vitro*, we incubated immunopurified KLHL6-Roquin2 complex with a ubiquitylation mix. High-molecular weight species of Roquin2 were detected with the KLHL6(WT) complex, but not with KLHL6(L65P) (Fig. 2k). Correspondingly, ubiquitylation of Roquin2 was abolished in *KLHL6*^{-/-} cell lines *in vivo* (Fig. S2h).

KLHL6 functions as a tumor suppressor in ABC-DLBCL by regulating its growth and survival

Although mutations of *KLHL6* occur at a similar rate in GCB- and ABC-DLBCL (Fig. 1B), low *KLHL6* expression correlated with a significantly poorer survival in ABC-DLBCL patients (Fig. 3a) as previously reported^{29, 30}.

To assess the biological effect of *KLHL6* loss in ABC-DLBCL lines, we infected Cas9-expressing U2932, OCI-LY10 and TMD8 cells with lentiviruses encoding three different gRNAs targeting the *KLHL6* gene locus. Ablation of *KLHL6* resulted in an increase in cellular proliferation and a decrease in apoptosis (Fig. 3b and 3c). This effect was confirmed in 3D cultures as measured by a larger number and size of colonies (Fig. S3a and S3b). To

rule out the possible off-target effects of gRNAs, we utilized shRNA-mediated knockdown of *KLHL6* in U2932 and OCI-LY10 and observed similar results (Fig. S3c–f).

To investigate the role of cancer mutations in cell growth, we re-expressed KLHL6(WT) or KLHL6 BTB-domain mutants or an empty vector (EV) in a clonally-derived U2932 *KLHL6*^{-/-} cell line (Fig. 3d). While re-expression of KLHL6(WT) decreased cell proliferation, expression of KLHL6 BTB-domain mutants phenocopied loss of *KLHL6*, confirming these mutations as loss of function. In xenograft models, expression of KLHL6(WT) decreased tumor burden while expression of KLHL6(S94I) displayed a similar tumor burden compared to *KLHL6*^{-/-} cells (EV) (Fig. 3e).

A non-degradable Roquin2 mutant phenocopies loss of KLHL6

We mapped the KLHL6 binding motif in Roquin2. By performing mutagenesis experiments, we identified a region in Roquin2 between amino acids 640 and 700 as necessary for interaction with KLHL6 (Fig. 4a and 4b). More refined deletions narrowed the interaction domain between amino acids 690 and 695 (Fig. 4c). Alanine scanning mutagenesis of the individual residues surrounding the 691-704 region revealed that a conserved tyrosine residue, in position 691, was required for KLHL6-Roquin2 interaction (Fig. 4d). *In vitro* binding assays confirmed that a Roquin2 peptide from 686 to 700 directly interacts with KLHL6 (Fig. S4a–d). Mutations of tyrosine 691 into alanine or phenylalanine impaired the ability of Roquin2 to co-immunoprecipitate with KLHL6 *in vivo* and *in vitro* (Fig. 4e and S4c), suggesting that the integrity of the tyrosine hydroxyl group is critical for KLHL6 interaction.

We retrovirally-transduced BJAB with Roquin2(WT) or Roquin2(Y691F) to investigate whether tyrosine 691 controls Roquin2 stability in DLBCL cells. Roquin2(Y691F) displayed increased protein levels at steady state as well as an extended half-life when compared to that of Roquin2(WT) (Fig. 4f and S4e). Furthermore, KLHL6(WT) effectively down-regulated protein levels of Roquin2(WT), but not those of Roquin2(Y691F) (Fig. S4f). KLHL6 BTB-mutant(L65P) had no effect on protein levels of Roquin2(WT) and Roquin2(Y691F) (Fig. S4f).

Next, we analyzed the effect of Roquin2 stabilization on DLBCL growth. Expression of the non-degradable Roquin2(Y691F) mutant increased tumor burden as monitored by tumor volume and weight at the experimental endpoint (Fig. 4g). This effect was not an artifact of overexpression because the levels of Roquin2(Y691F) were comparable to those of endogenous Roquin2 in *KLHL6*^{-/-} cells (Fig. S4g). Moreover, knockdown of Roquin2 impaired the cell growth advantage of *KLHL6*^{-/-} U2932 and OCI-LY10 cells (Fig. 4h, and S4h and S4i). Importantly, loss of Roquin2 increased toxicity of *KLHL6*^{-/-} cells preferentially (Fig. S4h), suggesting that loss of *KLHL6* promotes cell proliferation in a Roquin2-dependent manner.

KLHL6 is a BCR/NF- κ B target gene that links Roquin2 degradation to BCR signaling

KLHL6 is a member of the B-cell Receptor (BCR)-signalosome³¹ and is induced upon antigen stimulation in the germinal center³. Thus, we investigated whether mRNA and protein levels of KLHL6 and Roquin2 were affected by BCR stimulation. First, we found

ABC-DLBCL cells predominantly expressed an IgM-BCR as opposed to GCB-DLBCL cells, which are positive for IgG-BCR (Fig. S5a)³². Then, we analyzed levels of KLHL6 and Roquin2 in IgM-positive ABC-DLBCL cell lines (U2932, OCI-LY10 and HBL1) (Fig 5a). BCR stimulation using the fragment affinity-purified antibody F(ab')₂-IgM induced up-regulation of KLHL6 and a corresponding down-regulation of Roquin2 protein levels in OCI-LY10 and U2932, but not in HBL1 [cell line with low KLHL6 for both mRNA and protein levels (Fig. 5a)].

To demonstrate that BCR-dependent down-regulation of Roquin2 protein depends on CRLs, we pre-treated U2932 cells with MLN4924, a NEDD8-activating enzyme (NAE) inhibitor that blocks Cullin neddylation³³. MLN4924 treatment rescued Roquin2 down-regulation induced by BCR-crosslinking, suggesting that a functional CRL-complex is required to promote Roquin2 degradation (Fig. 5b). Notably, BCR stimulation induced KLHL6 up-regulation both at transcriptional and protein levels (Fig. 5a, 5b and 5c).

Since BCR signaling converges on NF- κ B activation¹⁰, we investigated whether *KLHL6* is an NF- κ B target gene. Analysis of CHIP-Seq datasets of NF- κ B factors³⁴ revealed enrichment of p50, p52, RelA and RelB at the *KLHL6* gene locus (Fig. 5d). Correspondingly, treatment of cells with an IKK or a BTK inhibitor (ibrutinib)¹³, resulted in a down-regulation of KLHL6 both at mRNA and protein levels (Fig. 5e). Interestingly, a reduced sensitivity of *KLHL6*^{-/-} cells to ibrutinib was observed (Fig. S5b).

BCR-induced Roquin2 degradation was impaired in *KLHL6*^{-/-} (Fig. 5f) and KLHL6-knockdown cells (Fig. S5c and S5d). Correspondingly, while exogenous Roquin2(WT) was degraded in a dose-dependent manner upon BCR stimulation, Roquin2(Y691F) mutant was not affected (Fig 5g), supporting BCR signaling promotes Roquin2 degradation in a KLHL6-dependent manner.

Stabilization of Roquin2 down-regulate BCR responsive genes

To investigate whether the pro-proliferative effect of the non-degradable Roquin2(Y691F) mutant depends on its RNA binding ability, we generated a double mutant Roquin2(Y691F ROQ) lacking the ROQ domain. Notably, deletion of the ROQ domain abolished the growth advantage induced by Roquin2(Y691F) expression (Fig. 6a).

Next, we investigated whether misregulation of Roquin2 degradation would result in a deregulation of the BCR transcriptional program. We measured differential gene expression in U2932 cells expressing Roquin2(WT) or Roquin2(Y691F) upon BCR ligation via RNA-seq (Fig. 6b and Supplementary Table 3). Pairwise comparison revealed that 133 mRNAs were significantly down-regulated in Roquin2(Y691F) expressing cells as compared to Roquin2(WT). 64 of these 133 mRNAs overlapped with BCR-responsive genes defined as those with at least a two-fold up-regulation in expression upon BCR stimulation in cells expressing Roquin2(WT) (Fig. 6b and 6c). These 64 genes represented BCR responsive genes that failed to be up-regulated upon BCR stimulation in presence of a non-degradable Roquin2 mutant.

Gene ontology (GO) enrichment analysis (Fig. S6a and Supplementary Table 4) revealed Roquin2 regulated genes are involved in immune and inflammatory responses and implicated as regulators of the NF- κ B pathway and lymphoid tumor suppressors (e.g., *TNF*, *NFKBIE*, *TNFAIP3*, *LTA*, *TNFRSF14*)^{14, 35–38}. To identify targets relevant to DLBCL biology, we ranked these genes by the percentage of genetic alterations in human DLBCL (TCGA, <http://cancergenome.nih.gov/>) and the base mean expression in our RNA-Seq analysis (Fig. S6b and Supplementary Table 3). We validated the top 11 candidates in a secondary screen and found 7 of them were dependent on a functional ROQ domain (Fig. S6b and c).

Amongst these targets, we focused on tumor necrosis factor- α -inducible gene 3 (*TNFAIP3*) because it is frequently inactivated in ABC-DLBCLs^{12–15} and is a direct target of the Roquin proteins¹⁹. We found that *TNFAIP3* was up-regulated upon BCR stimulation consistent with its function as a negative regulator of the NF- κ B program (Fig. 6d)³⁹. This response was abolished in cells expressing Roquin2(Y691F), suggesting that stabilization of Roquin2 contributes to a reduction of *TNFAIP3* mRNA levels during BCR signaling. This effect was rescued partially in cells expressing Roquin2(Y691F ROQ) as a build-up of *TNFAIP3* mRNA levels was observed. Notably, other NF- κ B target genes (*NFKBIE* and *LTA*) and the tumor suppressor gene *TNFRSF14* displayed a similar pattern.

Lastly, we investigated whether the KLHL6-Roquin2 axis directly controls *TNFAIP3* mRNA stability. Ablation of KLHL6 shortened the half-life of *TNFAIP3*, which was partially rescued by concomitant ablation of Roquin2 (Fig. 6e). Re-expression of KLHL6(WT) in VAL, which carries endogenous BTB-mutations, also increased the half-life of *TNFAIP3* (Fig. 6e).

KLHL6-Roquin2 axis controls NF- κ B activation

Since KLHL6 regulates *TNFAIP3* mRNA levels, we hypothesized that loss of *KLHL6* would lead to increased NF- κ B activation in ABC-DLBCL. First, we investigated whether the *TNFAIP3* transcriptional changes would reflect similar changes in protein levels. BCR dependent degradation of Roquin2(WT) inversely correlated with the up-regulation of TNFAIP3 levels, which was reduced in cells stably expressing Roquin2(Y691F) (Fig. 7a). Correspondingly, TNFAIP3 protein levels were down-regulated in *KLHL6*^{-/-} cells, both at steady state and in response to BCR stimulation (Fig. 7b). Knockdown of Roquin2 in U2932 *KLHL6*^{-/-} cells rescued TNFAIP3 levels similar to those of *KLHL6*^{+/+} cells (Fig. S7a). Likewise, depletion of Roquin2 more robustly upregulated of TNFAIP3 protein levels in HBL1 cells (Fig. 7c). Correspondingly, re-expression of KLHL6(WT) in U2932 *KLHL6*^{-/-} cells increased TNFAIP3 levels (Fig. S7b).

Next, we investigated whether loss of *KLHL6* resulted in increased IKK activation. The amount of I κ B α phosphorylation upon BCR stimulation was higher in *KLHL6*^{-/-} cells, suggesting increased IKK activity (Fig. 7d). Importantly, the increase in phosphorylation was reduced by re-expression of KLHL6(WT) (Fig. S7c). We also detected an increase in the nuclear translocation of the NF- κ B transcriptional factors in *KLHL6*^{-/-} cells (Fig. 7e), which was partially mitigated by the concomitant knockdown of Roquin2 (Fig. S7d).

Moreover, ablation of *KLHL6* increased RelA DNA-binding at the *NFKBIA* promoter, an effect reversed by simultaneous knockdown of Roquin2 (Fig. 7f).

We analyzed the mutual exclusivity of BTB-associated *KLHL6* mutations with *TNFAIP3* alterations in DLBCL patients. Deleterious *KLHL6* BTB-mutations showed no overlap with *TNFAIP3* biallelic deletion or mutation (Fig. 7g and S7e). Using a weighted test⁴⁰, we found exclusivity with a trend toward significance (*P*-value 0.085, Supplementary Table 5). Instead, 4 BTB-mutations had a coincident monoallelic deletion in *TNFAIP3*, suggesting that these mutations might confer additional NF- κ B activation when only one *TNFAIP3* allele is lost. Interestingly, tumour cells from patients with *KLHL6* mutations revealed a higher NF- κ B activity, although this signature was not only confined to *KLHL6* mutated cases (Fig. S7f).

To investigate whether the tumor suppressor role of *KLHL6* would be diminished in *TNFAIP3*-null ABC-DLBCLs, we ablated *KLHL6* in RCK8 cells¹⁴ and observed no significant effects on cellular proliferation (Fig. 7h) and apoptosis (Fig. 7i). Additionally, utilizing shRNAs targeting Roquin2 in both HBL1 (*TNFAIP3* WT) and HLY1 cells (*TNFAIP3*-null⁴¹), we observed elevated apoptosis in HBL1 only (Fig. 7j), indicating the relevance of Roquin2 in cells harboring a functional *TNFAIP3* gene.

Discussion

KLHL6 is a BTB-Kelch domain protein mutated in human DLBCL. Somatic mutations localize to the BTB domain with relevant hotspots at amino acids 65 and 90⁴⁻⁷. Most *KLHL6* alterations in DLBCL include monoallelic missense mutations and infrequent copy loss⁴⁻⁷. Mutations of *KLHL6* are likely the consequence of aberrant hypersomatic mutation⁴², similarly to those of *BCL6* and *MYC*⁴³. Importantly, the hotspots and other deleterious BTB-domain mutations result in loss of both CULLIN3 interaction and E3 ligase activity. Data from VAL cells suggest that mutations might be accompanied by a transcriptional down-regulation, resulting in a loss of function. Indeed, about 6% of DLBCL tumors display down-regulation of *KLHL6* transcript. In ABC-DLBCL cell lines, ablation of *KLHL6* promotes cell growth both *in vitro* and *in vivo*, supporting a tumor suppressor role. These findings are consistent with low *KLHL6* expression levels correlating with poorer survival in ABC-DLBCL patients^{29, 30}.

Furthermore, we identified Roquin2 as the bona fide substrate of *KLHL6*. *KLHL6* specifically binds, ubiquitylates and triggers Roquin2 (but not Roquin1) degradation in a BCR-dependent manner. Expression of a non-degradable Roquin2(Y691F) mutant phenocopies loss of *KLHL6* and concomitant ablation of Roquin2 in *KLHL6*^{-/-} cells results in an inhibition of cell proliferation. This pro-proliferative effect depends on the ability of Roquin2 to bind RNA¹⁸⁻²². Although Roquin1 and Roquin2 are genetically redundant in the T-cell compartment²¹, no studies have assessed the functional redundancy in B-cell cancers. Transgenic mice overexpressing Roquin2 or the non-degradable mutant in the GC might be helpful to model the oncogenic role of Roquin2 in DLBCL *in vivo*.

TNFAIP3 is a relevant target of Roquin2-mediated mRNA decay¹⁹. In ABC-DLBCL, BCR-signaling triggers transcription of *KLHL6* and degradation of Roquin2, thus releasing *TNFAIP3* from mRNA decay. We speculate that *KLHL6* inhibits *TNFAIP3* decay via Roquin2 degradation contributing in establishing a negative feedback loop to terminate the NF- κ B signaling (Fig. 7k). Thus, loss of *KLHL6* function promotes BCR-dependent activation of NF- κ B in ABC-DLBCL. Correspondingly, mutations of *KLHL6* correlate with high NF κ B signatures and could serve as a marker of resistance to NF κ B pathway targeting drugs such as Ibrutinib¹³, MLN4924³³ or bortezomib¹.

TNFAIP3 genetic mutations and deletions are frequently observed in ABC-DLBCLs^{12–15}. Functional reconstitution of *TNFAIP3* in *TNFAIP3*-null DLBCL causes apoptosis and growth arrest, supporting a tumor suppressor role in DLBCL^{44, 45}. Interestingly, co-occurrence of *KLHL6* BTB-mutations and *TNFAIP3* biallelic deletion or mutations was rarely observed in human DLBCL, suggesting that these two genes may have similar downstream components (*i.e.* IKK activation). A partial overlap between *KLHL6* BTB-mutations and *TNFAIP3* monoallelic deletion further points to a possible synergy towards NF- κ B activation. On the other hand, neither Roquin2 amplification nor sequence alteration of *TNFAIP3* mRNA at the Roquin2 binding site has been observed in DLBCLs. This suggests that the tumor suppressor mechanism of *KLHL6* might extend beyond Roquin2/*TNFAIP3* deregulation. It is possible that *KLHL6* might be involved in other biological processes such as cell adhesion, migration or immune surveillance in patients.

Much remains in evaluating the functional impact of the *KLHL6*-Roquin2 axis in GCB-DLBCLs, where unknown *KLHL6* substrates or different Roquin2 mRNA targets can contribute to the proliferation and survival of GCB-DLBCL cells. It is also worth noting that *KLHL6* mutations are not observable at high frequency in non-B-cell cancers, suggesting a possibly differential role for *KLHL6* in a different genetic and cellular context.

METHODS

Cell culture and drug treatment

HEK293T cells were maintained in Dulbecco's modified Eagle's medium containing 10% fetal bovine serum (FBS). U2932, BJAB, SUDHL4, SUDHL6, RAMOS, TMD8, HBL1, Pfeiffer, OCI-LY8, Karpas422, ARP1, RCK8, HLY-1, SUDHL10 and VAL were maintained in RPMI 1640 medium containing 10% FBS. OCI-LY1, OCI-LY7, OCI-LY10, and OCI-LY19 were maintained in Iscove's modified Dulbecco's Medium containing 10% FBS. For BCR-crosslinking experiment, Goat-F(ab')₂ anti-human IgM (SouthernBiotech, #2022-01) was used at indicated concentrations. For 3D matrigel colony formation assay, 150 μ l of Corning Matrigel Basement Membrane Matrix was used in mix of 100 μ l of DMEM/F12 containing 10% Knockout Serum Replacement (SR) and plated in Millicell EZ slide (Millipore). For quantification of cell numbers from colonies grown for 14 days, 300 μ l of Corning Dispase(#354235) was used according to manufacturers' protocols. The following drugs were used: proteasome inhibitor MG132 (Peptide Institute Inc.; 10 μ M final concentration), Cycloheximide (Sigma Aldrich; 50 μ g/ml final concentration), MLN4924 (Active Biochem; 5 μ M final concentration), IKK-16(Selleckchem; 10 μ M final concentration), Ibrutinib((Selleckchem; 5 μ M final concentration), ActinomycinD (Sigma

Aldrich; 2 μ g/ml final concentration), Doxycycline hyclate(Sigma Aldrich; 1 μ g/ml final concentration). When indicated, cells were selected with puromycin(Sigma Aldrich; 0.5 μ g/ml-1 μ g/ml final concentration) and hygromycin(ThermoFisher; 100 μ g/ml). MTS assays (Promega, G5421), AnnexinV staining (Thermo fisher Annexin V, Alexa Fluor® 680 conjugate; A35109) was performed according to manufacturers' protocols. For detection of IgM and IgG surface expression, FITC mouse anti-human IgM (BD, #562029) and APC mouse anti-human IgG (BD, #562025) were used according to manufacturing instruction.

Biochemical methods—Extract preparation, immunoprecipitation, and immunoblotting, fractionation of DLBCLs and chromatin immunoprecipitation were carried out according to ref⁴⁶. Bands quantification was performed using ImageJ software and plotted using nonlinear-fit curve in Prism. All antibodies were used at a dilution of 1:1000 unless specified. The following antibodies were used: anti-FLAG (Sigma, F7425, 1:3000), anti-HA (Biolegend, #901513), anti-Cullin1 (Invitrogen, #71-8700), anti-Cullin3 (Bethyl Laboratories, A301-109A), anti-ubiquitin K48 (EMD Millipore, 05-1307), anti-Roquin1/2 (EMD Millipore, MABF288), anti-Roquin2(Santa Cruz, sc-165026) anti-Roquin2(Bethyl Laboratories, A305-150A) anti-KLHL6 (Abcam, ab182163), anti-KLHL6(Novus Biologicals, NBP1-46128) anti-Tubulin(Santa Cruz, sc-8035), anti-GAPDH(EMD Millipore, MAB374, 1:5000), anti-CDK1(Santa Cruz, sc-954), anti-CDK2(Santa Cruz, sc-163), anti-p-AKT S473 (Cell Signaling Technology, #4051), anti-p-ERK T202/Y204 (Cell Signaling Technology, #9101), anti-ERK1/2 (Cell Signaling Technology, #9102), anti-AKT (Cell Signaling Technology, #4691), anti-TNFAIP3(Cell Signaling Technology, #5630), anti-p-I κ B S32 (Cell Signaling Technology, #2859, 1:500), anti-p100/p52(Cell Signaling Technology, #4882), anti-p105/p50(Santa Cruz, sc-7178), anti-RelA(Santa Cruz, sc-372), anti-RelB(Santa Cruz, sc-226), anti-histone H2A(EMD Millipore, 07-146) and anti-histone H3(Abcam, ab1791, 1:5000), ECL Rabbit IgG HRP-linked whole antibody(GE healthcare, NA934-1ML, 1:5000), ECL Mouse IgG, HRP-linked whole antibody(GE healthcare, NA931-1ML, 1:5000), Anti-Rat IgG (H+L) polyclonal antibody(Jackson Immunoresearch, 112-035-003, 1:5000), Anti-Goat IgG (H+L) polyclonal antibody(Jackson Immunoresearch, 705-035-003, 1:5000). KLHL6, Roquin1/2, TNFAIP3, CULLIN1, CULLIN3, p100/p52, p105/p50 and RelA antibodies were validated in our lab utilizing RNAi as well as overexpression, and were also validated by manufacturer. All other primary antibodies were validated on manufacturer datasheets.

The following agarose beads were used: anti-FLAG-M2 affinity gel (Sigma, A2220) and Strep-Tactin Superflow 50% suspension (Neuromics).

Xenotransplantation experiments—All animal work was performed following the ethical guidelines and protocols approved by the Institutional Animal Care and Use Committee of the University of Pennsylvania. NOD/SCID/IL2R $\gamma^{-/-}$ (NSG) mice were purchased from the Jackson Laboratory. Six to eight-week-old NSG mice received subcutaneous (s.c.) flank injections of 1×10^7 U2932 KLHL6 $^{-/-}$ (clone-derived) cells re-expressed either with empty vector, KLHL6(WT), or KLHL6(S94I), and 1×10^7 U2932 cells infected with retroviruses encoding HA-Roquin2(WT) or HA-Roquin2(Y691F) in 100 μ l sterile PBS. Tumor burden was monitored weekly by palpation and eye inspection. Tumor

volume calculated by caliper measurement. Tumor weight was analyzed on the excised tumors at the experimental endpoint using an analytical scale. After about one month, tumor volume and weight were measured.

Purification and analysis of KLHL6 interactors—Approximately 5×10^8 HEK293T and ARP-1 cells stably expressing FLAG-tagged KLHL6(WT) or FLAG-tagged KLHL6(L65P) cells were harvested and subsequently lysed in lysis buffer (LB: 50 mM Tris-HCl pH 7.5, 150 mM NaCl, 1 mM EDTA, 50 mM NaF, 0.5% NP40, plus protease and phosphatase inhibitors). KLHL6 was immunopurified with an anti-FLAG agarose resin (Sigma) and washed five times with LB (15 minutes each). After washing, proteins were eluted with FLAG peptides (Sigma). The eluates (1% of the IP) were separated by SDS-PAGE, and proteins were stained by Silver Staining (Life Technology). The final eluate was then precipitated with trichloroacetic acid (TCA).

In vitro ubiquitylation assay—The ubiquitylation of KLHL6 and Roquin2 was performed in a volume of 10 μ l, containing 50 mM Tris pH 7.6, 5 mM MgCl₂, 2 mM ATP, 1.5 ng/ μ l E1 (Boston Biochem), 10 ng/ μ l UBCH5C, 2.5 μ g/ μ l ubiquitin (Sigma), 1 μ M ubiquitin aldehyde, and purified FLAG-KLHL6 or FLAG-KLHL6/HA-Roquin2 complex from HEK293T cells via FLAG immunoprecipitation. The reactions were incubated at 37°C for the indicated times, subjected to SDS-PAGE, then analyzed by immunoblot. When indicated, upon reaction, beads were resuspended in 1% SDS, boiled, then diluted to 0.1% SDS. The eluted proteins were further FLAG-immunoprecipitated, washed and eluted in Laemmli buffer before SDS-PAGE analysis.

In vivo ubiquitylation assay—U2932 *KLHL6*^{+/+} and *KLHL6*^{-/-} (clone-derived) cells were treated with or without MG132 for 6hrs and lysed in 1% SDS. Lysates were then diluted to 0.1% SDS in NP-40 buffer and immunoprecipitated (IP) with a polyclonal antibody against Roquin2. The immunocomplexes were subjected to SDS-PAGE and analyzed by immunoblot.

In vitro binding assays—For *in vitro* binding assays, *in vitro*-translated FLAG-tagged KLHL6 was added to lysis buffer (50 mM Tris-HCl pH 7.5, 250 mM NaCl 0.1% Triton X-100, 1 mM EGTA) with indicated amounts of Roquin2 peptides. Anti-streptavidin resin was then added to the lysis buffer and incubated at 4°C for 2hrs. Samples were washed three times with the lysis buffer, and complexes were eluted in Laemmli buffer. For the use of HEK293T cells stably expressing KLHL6(WT), cells were lysed with the lysis buffer and anti-streptavidin resin was directly added to the whole cell lysates with the peptides.

Transient transfections and retrovirus-mediated gene transfer—HEK293T cells were transfected using polyethylenimine (PEI). For retrovirus and lentivirus production, GP-293 packaging cells (Clontech) or pCMV-DeltaR8.2 were used respectively. The virus-containing medium was collected after forty-eight hours of transfection and supplemented with 10 μ g/ml polybrene (Sigma). Then, cells were spin-infected at 1800rpm for 30 minutes with the viral supernatant for six hours to overnight. For RCK8, cells were electroporated using Neon transfection system according to manufacture's protocol with LentiCRISPRv2

vector carrying a GFP marker. Transfected cells were sorted by GFP. siRNA oligos transfection was performed with Neon transfection system.

Generating clonal *KLHL6*^{-/-} cell lines—U2932 or OCI-LY10 Cas9-expressing cells were infected with lentiviruses encoding gRNAs targeting the *KLHL6* exon1. Upon infection and puromycin selection, cells were plated in a 96 well plate at a concentration of 0.5 cells/well. Single clones were screened for *KLHL6* expression by immunoblotting.

Plasmids—Human Roquin1 and Roquin2 cDNA were kindly provided by Dr. Carola Vinuesa and subcloned into pcDNA3.1-FLAG, pcDNA3.1-HA or pcDNA3.1-FLAG-Streptavidin. Human *KLHL6* cDNA was purchased from Dharmacon and subcloned into pcDNA3.1-FLAG, pcDNA3.1-FLAG-Streptavidin, pREV-TRE. C-terminal deletion mutants and point mutants were generated by utilizing the QuikChange Site-directed Mutagenesis kit (Stratagene), and N-terminal deletion mutants were generated by standard PCR methods. For retrovirus production, cDNAs encoding FLAG-tagged or HA-tagged *KLHL6* and *KLHL6* mutants were subcloned into the retroviral vector MIGR1 and pREV-TRE vector. cDNAs encoding FLAG-HA-tagged or untagged Roquin2 and Roquin2 mutants were subcloned into the retroviral vector pBabe Puro or pMSCV. Lentivirus encoding shRNAs targeting human *KLHL6* were subcloned in pSicoR-Puro. Lentivirus encoding shRNAs targeting human Roquin2 were subcloned in pSicoR-GFP.

KLHL6 cDNA was clone into pTRIPZ using AgeI and HpaI.

The target sequences used to knock-down human *KLHL6* were:

h*KLHL6*_shRNA#1:

For:

TGCAGCCAGCAACTATTTTCATTCAAGAGATGAAATAGTTGCTGGCTGCTTTT
TTC

Rev:TCGAGAAAAAAGCAGCCAGCAACTATTTTCATCTCTTGAATGAAATAGT
TGCTGGCTGCA

h*KLHL6*_shRNA#2:

For:

TGAAGCCTTGAACCCAGAAATTCAAGAGATTTCTGGGTTCAAGGCTTCTTT
TTTC

Rev:TCGAGAAAAAAGAAGCCTTGAACCCAGAAATCTCTTGAATTTCTGGGT
TCAAGGCTTCA

h*KLHL6*_shRNA#3:

For: TGCATGATGTTTGGAAATAT

TTCAAGAGAATATTTCCAAACATCATGCTTTTTTC

Rev:TCGAGAAAAA GCATGATGTTTGGAAATAT
TCTCTTGAATATTTCCAAACATCATGCA

hKLHL6_shRNA#4:

For: TGGATTCAGATTGAGTATTT
TTCAAGAGAAAATACTCAATCTGAATCCTTTTTTC

Rev:TCGAGAAAAAA GGATTCAGATTGAGTATTT
TCTCTTGAAAAATACTCAATCTGAATCCA

The target sequences used to knock-down human Roquin2 were:

hRoquin2 shRNA#1:

For :
TGCAGTTGTCTGCCAATCTATTCAAGAGATAGATTGGCAGACAACACTGCTTTT
TTC

Rev:TCGAGAAAAAAGCAGTTGTCTGCCAATCTATCTCTTGAATAGATTGGC
AGACAACACTGCA

hRoquin2 shRNA#2:

For:
TGGACTCAGATACCCTTTGATTCAAGAGATCAAAGGGTATCTGAGTCCTTTT
TTC

Rev:TCGAGAAAAAAGGACTCAGATACCCTTTGATCTCTTGAATCAAAGGGT
ATCTGAGTCCA

Lentiviruses encoding gRNAs targeting human KLHL6 were subcloned into Lenti-Guide-Puro vector, Lenti-Guide-GFP and LentiCRISPRv2 vector. The target sequences to knockout human KLHL6 were:

hKLHL6_gRNA#2 For: CAGAGCGTTTTCCATTGCA
Rev: TGCGAATGGAAAACGCTCTG

hKLHL6_gRNA#3 For: TCAGAGCGTTTTCCATTGCG
Rev: GCGAATGGAAAACGCTCTGA

hKLHL6_gRNA#4 For: AAAGGTCAAATTTGACGACG
Rev: CGTCGTCAAATTTGACCTTT

hKLHL6_gRNA#5 For: GACTTGGTCGAGATCTTAAA
Rev: TTAAAGATCTCGACCAAGTC

hKLHL6_gRNA#6 For: ACTTGGTCGAGATCTTAAAT
Rev: ATTTAAGATCTCGACCAAGT

Gene silencing by siRNA—For siRNA-mediated silencing, duplexes were purchased from Dharmacon. The target sequence for human KLHL6 siRNA was GCACGAAGGAUGAACGGUU, The target sequence for human Roquin2 siRNA was GCUUGAAAAGUAUCGAUUA. Non-targeting siRNA control sequence was UGGUUUACAUGUCGACUAA.

mRNA Analysis—RNA was extracted using the RNeasy Kit (Qiagen) and trizol(Invitrogen). cDNA synthesis was performed using Maxima first strand cDNA

synthesis kit (Thermo Fisher) and RNA to cDNA Ecodry Premix kit(Clontech). Quantitative PCR analysis with SYBR Green PCR Master Mix (Applied Biosystems) was performed according to standard procedures. Primer sequences were:

<i>hGAPDH</i>	FOR: 5' GGAGCGAGATCCCTCCAAAAT 3'
	REV: 5' GGCTGTTGCATACTTCTCATGG 3'
<i>hTNFAIP3</i>	FOR: 5' TCCTCAGGCTTTGTATTGAGC 3'
	REV: 5' TGTGTATCGGTGCATGGTTTAA 3'
<i>hTNFRSF14</i>	FOR: 5' CCACTGGGTATGGTGGTTTC 3'
	REV: 5' TCACCTTCTGCCTCCTGTCT 3'
<i>hTNF</i>	FOR: 5' CTGCACTTGGAGTGATCGGC3'
	REV: 5' CACCAGCTGGTTATCTCTCAGCTCC 3'
<i>hNFKBIE</i>	FOR: 5' TCTGGCATTGAGTCTCTGCG 3'
	REV: 5' AGGAGCCATAGGTGGAATCAG 3'
<i>hLTA</i>	FOR: 5' GCTGCTGGTTCTGCTGCC 3'
	REV: 5' CAAGGAGAAACCATCCTGGAGGAAG 3'
<i>hNEDD4L</i>	FOR: 5' ACTTCCTCCTCCTCTCTGC 3'
	REV: 5' TCCAAGTCTTCGCTGATGTG 3'
<i>hABLIM1</i>	FOR: 5' ACTGCATCTCTCCCTGGCTA 3'
	REV: 5' TGTTGGTCACCATGAGCATT 3'
<i>hSYNGAPI</i>	FOR: 5' TCTGAGGAAAACCTGCGAGGT 3'
	REV: 5' GCAAACACCTCCTTCAGCTC 3'
<i>hNEIL2</i>	FOR: 5' GCCTCCACAAAAGAAGTGC 3'
	REV: 5' TTGTTGGCTTTCTTGGCTCT 3'
<i>hLGALS8</i>	FOR: 5' CTGGGCATTTATGGCAAAGT 3'
	REV: 5' GACAGTTCTGGGTGCGATT 3'
<i>hCD274</i>	FOR: 5' TATGGTGGTGCCGACTACAA 3'
	REV: 5' TGCTTGTCAGATGACTTCG 3'
<i>hKLHL6</i>	FOR: 5' GCAGCCAGCAACTATTCAGG 3'
	REV: 5' ACGTGTAGTCCAACAGAGTGT 3'
<i>hNFKBIA</i>	FOR: 5' TATAAACGCTGGCTGGG 3'
	REV: 5' CCCTAGTGGTCTCATCGC 3'

Normalization and quantification of protein levels—Protein concentrations of cell extracts were measured using a Bio-Rad DC protein assay (Lowry assay) according to the manufacturer's protocol. For each experiment, equal amounts of protein (~15µg) were separated by SDS-PAGE and analyzed by immunoblotting. Equal protein levels in each lane were confirmed by Ponceau S staining of the membrane and by immunoblotting a constitutively expressed protein.

Cell Proliferation Assay— 2×10^3 cells were plated for MTS assay according to manufacturers' protocols.

For the long-term cell proliferation assay, 5×10^4 - 2×10^5 cells were plated, counted and re-plated every 3–5 days.

Flow cytometry—Flow cytometry was performed on Attune NxT Flow Cytometer using FITC for GFP-expressing cells, Alexa-680 AnnexinV to detect apoptosis, FITC to detect IgM or APC to detect IgG staining. All stainings were performed according to manufacturers' protocols. For investigating shRNA or gRNA effects on survival, 5×10^5 cells were spin-infected in a 24-well plate with 1000 μ l lentivirus containing medium in the presence of polybrene (8 μ g/ml). Media was changed after the spin-infection and the number of infected cells was determined on day 2 when GFP was fully expressed in all infected cells. The number of viable GFP positive cells on day 2 was set to 100% to normalize for transduction efficiency and every consecutive assessment was calculated in relation to day 2. When indicated, AnnexinV positive cells were gated on GFP positive cells (see gating strategy in Supplementary Figures 3 and 5).

MudPIT analysis—TCA-precipitated proteins were urea-denatured, reduced, alkylated and digested with endoproteinase Lys-C (Roche), followed by modified trypsin (Roche), as described^{47, 48}. Peptide mixtures were loaded onto 100- μ m fused silica microcapillary columns packed with 5- μ m C18 reverse phase (Aqua, Phenomenex), strong cation exchange particles (Luna, Phenomenex), and reverse phase⁴⁹. Loaded microcapillary columns were placed in-line with a Quaternary Agilent 1100 series HPLC pump and a LTQ linear ion trap mass spectrometer equipped with a nano-LC electrospray ionization source (Thermo Scientific). Fully automated 10-step MudPIT runs were carried out on the electrosprayed peptides, as described⁴⁷. Tandem mass (MS/MS) spectra were interpreted using SEQUEST⁵⁰ against a database of 61,318 sequences, consisting of 30,449 non-redundant human proteins (downloaded from NCBI on 2012-08-27, 160 usual contaminants (such as human keratins, IgGs and proteolytic enzymes), and, to estimate false discovery rates, 30,659 randomized amino-acid sequences derived from each non-redundant protein entry. Peptide/spectrum matches were sorted and selected using DTASelect with the following criteria set: spectra/peptide matches were only retained if they had a Δ Cn of at least 0.08 and a minimum XCorr of 1.8 for singly-, 2.0 for doubly-, and 3.0 for triply-charged spectra. In addition, peptides had to be fully tryptic and at least seven amino acids long. Combining all runs, proteins had to be detected by at least two such peptides, or one peptide with two independent spectra. Under these criteria the final FDRs at the protein and spectral levels were $2.1\% \pm 0.3$ and $0.94\% \pm 0.03$, respectively. Peptide hits from multiple runs were compared using CONTRAST⁵¹. To estimate relative protein levels, Normalized Spectral Abundance Factors (NSAFs) were calculated for each detected protein, as described^{52,53,54}.

Analysis of KLHL6 expression in DLBCL patients—Raw DNA copy number data from high resolution single nucleotide polymorphism (SNP) microarray analysis of 609 primary DLBCL tumors were utilized from a previously published study²⁶. The data were visualized using the integrative genomics viewer (IGV)⁵⁵. Cases were sorted according to their KLHL6 copy number status, and those with copy number < 1.8 were classified as possessing a deletion, according to previously described criteria⁵⁶.

Gene expression microarray from 249 tumors with matched DNA copy number data were obtained from a previously published study²⁶. Their cell of origin subtype was determined using the Wright algorithm⁵⁷, as previously reported⁵⁶. Row normalized heatmaps for 4

probe sets corresponding to KLHL6 were sorted according to their average expression, and significant reduction in KLHL6 expression defined as being 1 standard deviation below the mean.

Raw cel files for publicly available Affymetrix U133 plus 2.0 gene expression microarray data for diffuse large B-cell lymphoma tumors (GSE10846, GSE34171, GSE31312) were obtained from the gene expression omnibus. Data were RMA normalized using the ExpressionFileCreator module of GenePattern⁵⁸. Scores to categorize diffuse large B-cell lymphoma tumors by cell of origin subtype were calculated according to the Wright algorithm⁵⁷. Intensities from the 4 probes for KLHL6 (1555275_a_at, 1560396_at, 1560397_s_at, 228167_at) were averaged for use in the survival analysis. Cases were dichotomized into being above or below the median expression level of KLHL6 expression within each dataset to avoid confounding batch effects. For NF- κ B signatures, Affymetrix U133 plus 2 gene expression microarrays were performed on 84 matched DLBCL tumors^{26,59}. Raw cel files were RMA normalized with median scaling using the ExpressionFileCreator module of GenePattern⁵⁸. Sample-level enrichment of NF- κ B target genes was calculated using the single sample gene set enrichment analysis⁶⁰ and the c3 TFT gene set database of mSigDB⁶¹.

RNA-seq—Total RNA was extracted from U2932 cells using RNeasy Mini Kit (QIAGEN, #74104) and polyA+ transcripts isolated with oligo (dT)₂₅-conjugated magnetic Dynabeads (Thermo Fisher). Strand specific RNA-seq libraries were prepared following a published protocol⁶². Briefly, RNA was chemically fragmented in first strand buffer, converted to cDNA using SuperScript® III reverse transcriptase (Invitrogen), end-repaired, A-tailed and ligated to custom-designed universal adapters using an end-repair mix, klenow fragment, and T4 DNA ligase (all from Enzymatics). After ligation, adapters were removed by SPRI purification using SPRIselect beads (Beckman coulter) and amplified with Q5 Hot Start DNA polymerase (New England Biolabs) while introducing custom dual indexes. Three biological replicates were sequenced on a NextSeq 500 (Illumina) at a depth of at least 2×10^7 reads each. Reads were mapped and analyzed with a custom bioinformatic pipeline based on STAR⁶³, SAMTOOLS⁶⁴, and the R packages DEGseq⁶⁵ and DEseq2⁶⁶. We used human genome version GRCh38 and gene annotations from the ENSEMBL release 83. GO analyses were performed using version 6.8 of the DAVID web server^{67, 68}.

CHIP-seq—The data discussed in this publication were obtained from the NCBI's Gene Expression Omnibus³⁴ and are accessible through GEO at Series accession numbers GSE55105. FASTQs were downloaded and mapped to hg19 with bowtie2 (v2.1.0). Genome browser tracks were generated using custom scripts. When available, biological replicate were merged by taking the mean of the reads density at each position. The data were visualized using the integrative genomics viewer (IGV)⁵⁵.

Statistics and Reproducibility—All graphs show mean values with error bars signifying standard deviation (s.d.) as indicated in the figure legends. Exact P values for each experiment are provided in Supplementary Table 6. Unless otherwise noted, all immunoblots were successfully repeated at least three times. One-tailed *t*-test was performed for Fig. 3e (right panel) and two-tailed *t*-test for Fig 4g. Other analyses performed were

either one-way (Fig. 3c, 3e (left panel), 5e, 6a, 7i, 7j, S3b, S3f) or two-way ANOVA (Fig. 1i, 3b, 3d, 4g, 4h, 6e, 7h, S2d, S3d, S4e, S4h, S5b) as indicated in the figure legends. DEseq2 was performed for RNA-seq analysis in Fig. 6b and Supplementary Table 3. Weighted Exclusivity Test (WExT) was performed for Supplementary Table 5. Mantel-Cox was performed for survival analysis in Fig. 3a. Pearson Correlation Coefficient was used in Fig. S2c.

Data availability—RNA-seq data that support the findings of this study have been deposited in the Gene Expression Omnibus (GEO) under accession code GSE93675. Previously published CHIP-seq data were obtained from GEO under accession code GSE55105. *KLHL6* copy number change and expression were calculated through re-analysis of SNP data and microarray from GSE11318, GSE12906, GSE15127, GSE22082, GSE34171 and GSE11318, GSE34171, respectively. Microarray data for DLBCL survival were obtained from GEO under accession code GSE10846, GSE34171, GSE31312. Data for NF- κ B signature correlation were retrieved from GSE10846. Raw mass spectrometry data are available in PRIDE (<https://www.ebi.ac.uk/pride/archive/>) under accession code PXD008963.

Raw data from independent experiments with $n < 5$ can be found in the Statistical source data (Supplementary Table 6). Unprocessed immunoblots are provided in Supplementary Fig. 8. All other data supporting the findings of this study are available from the corresponding author on reasonable request.

Supplementary Material

Refer to Web version on PubMed Central for supplementary material.

Acknowledgments

The authors thank Dr. Carola Vinuesa for kindly providing Roquins cDNAs, Dr. Andrei Thomas-Tikhonenko, Dr. Laura Pasqualucci and Dr. Yibin Yang for kindly providing DLBCL cell lines, Dr. Michele Pagano for kindly providing FBPs cDNAs, Dr. Bangjin Kim for helping with 3D matrigel colony formation assay; Rizwan Saffie, Dr. Donita Brady, Dr. Eric Witze and Dr. Roger Greenberg for critically reading the manuscript. This work was supported in part by grant R00-CA166181-04, R01-CA207513-01 from the National Cancer Institute and Gilead Sciences Research Scholars Program in Hematology/Oncology to L.B. R.B. is supported by an NIH Innovator Award (DP2MH107055), the Searle Scholars Program (15-SSP-102), the March of Dimes Foundation (1-FY-15-344), and the W.W. Smith Charitable Trust (C1404).

References

1. Yang Y, Staudt LM. Protein ubiquitination in lymphoid malignancies. *Immunol Rev.* 2015; 263:240–256. [PubMed: 25510281]
2. Gupta-Rossi N, et al. Specific over-expression of deltex and a new Kelch-like protein in human germinal center B cells. *Mol Immunol.* 2003; 39:791–799. [PubMed: 12617994]
3. Kroll J, et al. The BTB-kelch protein KLHL6 is involved in B-lymphocyte antigen receptor signaling and germinal center formation. *Mol Cell Biol.* 2005; 25:8531–8540. [PubMed: 16166635]
4. Morin RD, et al. Frequent mutation of histone-modifying genes in non-Hodgkin lymphoma. *Nature.* 2011
5. Lohr JG, et al. Discovery and prioritization of somatic mutations in diffuse large B-cell lymphoma (DLBCL) by whole-exome sequencing. *Proc Natl Acad Sci U S A.* 2012; 109:3879–3884. [PubMed: 22343534]

6. Idoia GR, et al. CREBBP Loss Cooperates with BCL2 Over-Expression to Promote Lymphoma in Mice. *Blood*. 2016; 128
7. Reddy A, et al. Genetic and Functional Drivers of Diffuse Large B Cell Lymphoma. *Cell*. 2017; 171:481–494 e415. [PubMed: 28985567]
8. Alizadeh AA, et al. Distinct types of diffuse large B-cell lymphoma identified by gene expression profiling. *Nature*. 2000; 403:503–511. [PubMed: 10676951]
9. Rosenwald A, et al. Molecular diagnosis of primary mediastinal B cell lymphoma identifies a clinically favorable subgroup of diffuse large B cell lymphoma related to Hodgkin lymphoma. *J Exp Med*. 2003; 198:851–862. [PubMed: 12975453]
10. Staudt LM. Oncogenic activation of NF-kappaB. *Cold Spring Harb Perspect Biol*. 2010; 2:a000109. [PubMed: 20516126]
11. Young RM, Shaffer AL 3rd, Phelan JD, Staudt LM. B-cell receptor signaling in diffuse large B-cell lymphoma. *Semin Hematol*. 2015; 52:77–85. [PubMed: 25805587]
12. Lenz G, et al. Oncogenic CARD11 mutations in human diffuse large B cell lymphoma. *Science*. 2008; 319:1676–1679. [PubMed: 18323416]
13. Davis RE, et al. Chronic active B-cell-receptor signalling in diffuse large B-cell lymphoma. *Nature*. 2010; 463:88–U97. [PubMed: 20054396]
14. Compagno M, et al. Mutations of multiple genes cause deregulation of NF-kappaB in diffuse large B-cell lymphoma. *Nature*. 2009; 459:717–721. [PubMed: 19412164]
15. Kato M, et al. Frequent inactivation of A20 in B-cell lymphomas. *Nature*. 2009; 459:712–716. [PubMed: 19412163]
16. Fu M, Blakeshear PJ. RNA-binding proteins in immune regulation: a focus on CCCH zinc finger proteins. *Nat Rev Immunol*. 2016
17. Kataoka K, et al. Aberrant PD-L1 expression through 3'-UTR disruption in multiple cancers. *Nature*. 2016; 534:402–406. [PubMed: 27281199]
18. Leppik K, et al. Roquin promotes constitutive mRNA decay via a conserved class of stem-loop recognition motifs. *Cell*. 2013; 153:869–881. [PubMed: 23663784]
19. Murakawa Y, et al. RC3H1 post-transcriptionally regulates A20 mRNA and modulates the activity of the IKK/NF-kappaB pathway. *Nat Commun*. 2015; 6:7367. [PubMed: 26170170]
20. Glasmacher E, et al. Roquin binds inducible costimulator mRNA and effectors of mRNA decay to induce microRNA-independent post-transcriptional repression. *Nat Immunol*. 2010; 11:725–733. [PubMed: 20639877]
21. Vogel KU, et al. Roquin paralogs 1 and 2 redundantly repress the Icos and OX40 costimulator mRNAs and control follicular helper T cell differentiation. *Immunity*. 2013; 38:655–668. [PubMed: 23583643]
22. Schlundt A, et al. Structural basis for RNA recognition in roquin-mediated post-transcriptional gene regulation. *Nat Struct Mol Biol*. 2014; 21:671–678. [PubMed: 25026077]
23. Yu D, et al. Roquin represses autoimmunity by limiting inducible T-cell co-stimulator messenger RNA. *Nature*. 2007; 450:299–303. [PubMed: 18172933]
24. Puente XS, et al. Non-coding recurrent mutations in chronic lymphocytic leukaemia. *Nature*. 2015; 526:519–524. [PubMed: 26200345]
25. Lohr JG, et al. Widespread genetic heterogeneity in multiple myeloma: implications for targeted therapy. *Cancer Cell*. 2014; 25:91–101. [PubMed: 24434212]
26. Green MR, et al. Transient expression of Bcl6 is sufficient for oncogenic function and induction of mature B-cell lymphoma. *Nat Commun*. 2014; 5:3904. [PubMed: 24887457]
27. Lydeard JR, Schulman BA, Harper JW. Building and remodelling Cullin-RING E3 ubiquitin ligases. *EMBO Rep*. 2013; 14:1050–1061. [PubMed: 24232186]
28. Lo SC, Li XC, Henzl MT, Beamer LJ, Hannink M. Structure of the Keap1 : Nrf2 interface provides mechanistic insight into Nrf2 signaling. *Embo Journal*. 2006; 25:3605–3617. [PubMed: 16888629]
29. Leo Meriranta AP, Alejandra Cervera, Harald Holte Jr., Rainer Lehtonen, Sampsa Hautaniemi and Sirpa Leppä Low Expression and Somatic Mutations of the KLHL6 Gene Predict Poor Survival in Patients with Activated B-Cell like Diffuse Large B-Cell Lymphoma. *Blood*. 2016; 128(22):2926.

30. Kunder CA, et al. KLHL6 Is Preferentially Expressed in Germinal Center-Derived B-Cell Lymphomas. *Am J Clin Pathol*. 2017; 148:465–476. [PubMed: 29140403]
31. Satpathy S, et al. Systems-wide analysis of BCR signalosomes and downstream phosphorylation and ubiquitylation. *Mol Syst Biol*. 2015; 11:810. [PubMed: 26038114]
32. Lenz G, et al. Aberrant immunoglobulin class switch recombination and switch translocations in activated B cell-like diffuse large B cell lymphoma. *Journal of Experimental Medicine*. 2007; 204:633–643. [PubMed: 17353367]
33. Milhollen MA, et al. MLN4924, a NEDD8-activating enzyme inhibitor, is active in diffuse large B-cell lymphoma models: rationale for treatment of NF-kappa B-dependent lymphoma. *Blood*. 2010; 116:1515–1523. [PubMed: 20525923]
34. Zhao B, et al. The NF-kappa B Genomic Landscape in Lymphoblastoid B Cells. *Cell Reports*. 2014; 8:1595–1606. [PubMed: 25159142]
35. Zhou A, Scoggin S, Gaynor RB, Williams NS. Identification of NF-kappa B-regulated genes induced by TNFalpha utilizing expression profiling and RNA interference. *Oncogene*. 2003; 22:2054–2064. [PubMed: 12673210]
36. Tian B, Nowak DE, Jamaluddin M, Wang S, Brasier AR. Identification of direct genomic targets downstream of the nuclear factor-kappaB transcription factor mediating tumor necrosis factor signaling. *J Biol Chem*. 2005; 280:17435–17448. [PubMed: 15722553]
37. Mansouri L, et al. Frequent NFKBIE deletions are associated with poor outcome in primary mediastinal B-cell lymphoma. *Blood*. 2016; 128:2666–2670. [PubMed: 27670424]
38. Boice M, et al. Loss of the HVEM Tumor Suppressor in Lymphoma and Restoration by Modified CAR-T Cells. *Cell*. 2016; 167:405–418 e413. [PubMed: 27693350]
39. Chu YY, et al. B cells lacking the tumor suppressor TNFAIP3/A20 display impaired differentiation and hyperactivation and cause inflammation and autoimmunity in aged mice. *Blood*. 2011; 117:2227–2236. [PubMed: 21088135]
40. Leiserson MDM, Reyna MA, Raphael BJ. A weighted exact test for mutually exclusive mutations in cancer. *Bioinformatics*. 2016; 32:736–745.
41. Fontan L, et al. MALT1 Small Molecule Inhibitors Specifically Suppress ABC-DLBCL In Vitro and In Vivo. *Cancer Cell*. 2012; 22:812–824. [PubMed: 23238016]
42. Puente XS, et al. Whole-genome sequencing identifies recurrent mutations in chronic lymphocytic leukaemia. *Nature*. 2011; 475:101–105. [PubMed: 21642962]
43. Pasqualucci L, et al. Hypermutation of multiple proto-oncogenes in B-cell diffuse large-cell lymphomas. *Nature*. 2001; 412:341–346. [PubMed: 11460166]
44. Honma K, et al. TNFAIP3/A20 functions as a novel tumor suppressor gene in several subtypes of non-Hodgkin lymphomas. *Blood*. 2009; 114:2467–2475. [PubMed: 19608751]
45. Schmitz R, et al. TNFAIP3 (A20) is a tumor suppressor gene in Hodgkin lymphoma and primary mediastinal B cell lymphoma. *J Exp Med*. 2009; 206:981–989. [PubMed: 19380639]
46. Busino L, et al. Fbxw7alpha- and GSK3-mediated degradation of p100 is a pro-survival mechanism in multiple myeloma. *Nat Cell Biol*. 2012; 14:375–385. [PubMed: 22388891]
47. Florens L, Washburn MP. Proteomic analysis by multidimensional protein identification technology. *Methods Mol Biol*. 2006; 328:159–175. [PubMed: 16785648]
48. Washburn MP, Wolters D, Yates JR 3rd. Large-scale analysis of the yeast proteome by multidimensional protein identification technology. *Nat Biotechnol*. 2001; 19:242–247. [PubMed: 11231557]
49. McDonald WH, Ohi R, Miyamoto DT, Mitchison TJ, Yates JR. Comparison of three directly coupled HPLC MS/MS strategies for identification of proteins from complex mixtures: single-dimension LC-MS/MS, 2-phase MudPIT, and 3-phase MudPIT. *International Journal of Mass Spectrometry*. 2002; 219:245–251.
50. Eng JK, McCormack AL, Yates JR. An approach to correlate tandem mass spectral data of peptides with amino acid sequences in a protein database. *J Am Soc Mass Spectrom*. 1994; 5:976–989. [PubMed: 24226387]
51. Tabb DL, McDonald WH, Yates JR 3rd. DTASelect and Contrast: tools for assembling and comparing protein identifications from shotgun proteomics. *J Proteome Res*. 2002; 1:21–26. [PubMed: 12643522]

52. Florens L, et al. Analyzing chromatin remodeling complexes using shotgun proteomics and normalized spectral abundance factors. *Methods*. 2006; 40:303–311. [PubMed: 17101441]
53. Paoletti AC, et al. Quantitative proteomic analysis of distinct mammalian Mediator complexes using normalized spectral abundance factors. *Proc Natl Acad Sci U S A*. 2006; 103:18928–18933. [PubMed: 17138671]
54. Zybailov B, et al. Statistical analysis of membrane proteome expression changes in *Saccharomyces cerevisiae*. *J Proteome Res*. 2006; 5:2339–2347. [PubMed: 16944946]
55. Robinson JT, et al. Integrative genomics viewer. *Nat Biotechnol*. 2011; 29:24–26. [PubMed: 21221095]
56. Monti S, et al. Integrative analysis reveals an outcome-associated and targetable pattern of p53 and cell cycle deregulation in diffuse large B cell lymphoma. *Cancer Cell*. 2012; 22:359–372. [PubMed: 22975378]
57. Wright G, et al. A gene expression-based method to diagnose clinically distinct subgroups of diffuse large B cell lymphoma. *Proc Natl Acad Sci U S A*. 2003; 100:9991–9996. [PubMed: 12900505]
58. Reich M, et al. GenePattern 2.0. *Nat Genet*. 2006; 38:500–501. [PubMed: 16642009]
59. Lenz G, et al. Stromal gene signatures in large-B-cell lymphomas. *N Engl J Med*. 2008; 359:2313–2323. [PubMed: 19038878]
60. Barbie DA, et al. Systematic RNA interference reveals that oncogenic KRAS-driven cancers require TBK1. *Nature*. 2009; 462:108–U122. [PubMed: 19847166]
61. Liberzon A, et al. Molecular signatures database (MSigDB) 3.0. *Bioinformatics*. 2011; 27:1739–1740. [PubMed: 21546393]
62. Parkhomchuk D, et al. Transcriptome analysis by strand-specific sequencing of complementary DNA. *Nucleic Acids Res*. 2009; 37:e123. [PubMed: 19620212]
63. Dobin A, et al. STAR: ultrafast universal RNA-seq aligner. *Bioinformatics*. 2013; 29:15–21. [PubMed: 23104886]
64. Li H, et al. The Sequence Alignment/Map format and SAMtools. *Bioinformatics*. 2009; 25:2078–2079. [PubMed: 19505943]
65. Wang L, Feng Z, Wang X, Wang X, Zhang X. DEGseq: an R package for identifying differentially expressed genes from RNA-seq data. *Bioinformatics*. 2010; 26:136–138. [PubMed: 19855105]
66. Love MI, Huber W, Anders S. Moderated estimation of fold change and dispersion for RNA-seq data with DESeq2. *Genome Biol*. 2014; 15:550. [PubMed: 25516281]
67. Huang DW, Sherman BT, Lempicki RA. Systematic and integrative analysis of large gene lists using DAVID bioinformatics resources. *Nature Protocols*. 2009; 4:44–57. [PubMed: 19131956]
68. Huang DW, Sherman BT, Lempicki RA. Bioinformatics enrichment tools: paths toward the comprehensive functional analysis of large gene lists. *Nucleic Acids Research*. 2009; 37:1–13. [PubMed: 19033363]

- (b)** Percentage of *KLHL6* mutations in DLBCL subtypes. Cohorts from UNMC and CMSGSC were pooled and sub-classified as Activated B-cell-like (ABC)-, Germinal Center B-cell-like (GC)- and Uncharacterized-DLBCL.
- (c)** Schematic representation of *KLHL6* mutations (BTB, Broad-Complex, Tramtrack and Bric-a-brac; BACK, BTB and C-terminal Kelch plant homeodomain).
- (d)** Proteomic analysis of *KLHL6* complex. Spectral counts for CULLIN3 are shown. EV, empty vector. This analysis was performed once in HEK293T and ARP-1 cells.
- (e)** Immunoblot analysis of immunoprecipitated FLAG-tagged E3 ligases in HEK293T cells. WCL, whole cell lysates. EV, empty vector.
- (f)** *In vitro* ubiquitylation reaction of immunopurified FLAG-*KLHL6* and Kelch mutant.
- (g)** Immunoblot analysis of immunoprecipitated FLAG-tagged *KLHL6* wild-type (WT), BTB-mutants (L65P, S94I and F97L), or empty vector (EV) in HEK293T cells.
- (h)** *In vitro* ubiquitylation reaction of immunopurified FLAG-*KLHL6* wild-type (WT) and BTB-mutants (L65P, S94I and F97L).
- (i)** Immunoblot analysis of whole cell lysates from GFP⁺ OCI-Ly10 *KLHL6*^{-/-} cells (clone-derived) retrovirally transduced with cDNAs encoding an empty vector (EV), *KLHL6*(WT) or BTB-mutants (L65P, S94I and F97L) and carrying a GFP marker (left panel). Cells were treated with cycloheximide (CHX) for the indicated times. Right panel shows quantification of *KLHL6* protein levels (mean±s.d., n=3 independent experiments, two-way ANOVA, *** P value 0.001; ****P value 0.0001).
- (j)** Schematic model of Cullin3-Ring-Ligase (CRL3)-*KLHL6* complex.
- Unprocessed original scan of immunoblots for *(e,f,g,h,i)* are shown in Supplementary Fig. 8, and statistical source data and exact P values for *(i)* can be found in Supplementary Table 6. Unless otherwise noted, immunoblots are representative of three independent experiments.

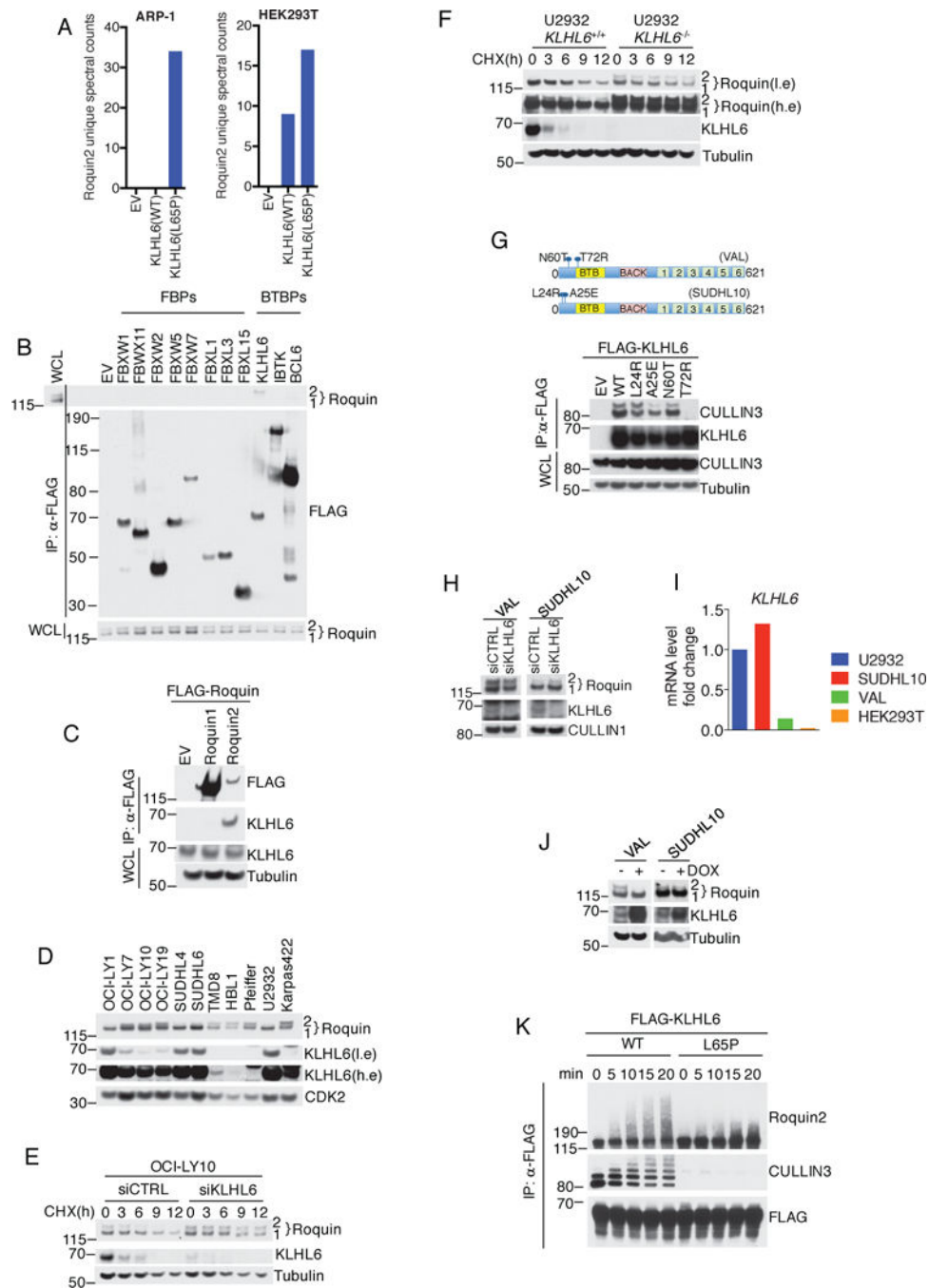


Figure 2. KLHL6 interacts and promotes ubiquitylation and degradation of Roquin2
(a) Proteomic analysis of KLHL6 immunoprecipitations. Spectral counts for Roquin2 proteins are shown. EV, empty vector. The analysis was performed once in two different cell lines (HEK293T and ARP-1).
(b) Immunoblot analysis of immunoprecipitated FLAG-F-box proteins (FBPs) or BTB proteins (BTBPs) in HEK293T cells. Lane 1 shows whole cell lysates (WCL) from cells transfected with an empty vector.

- (c)** Immunoblot analysis of immunoprecipitated FLAG-Roquin1 or FLAG-Roquin2 in HEK293T cells.
- (d)** Immunoblot analysis of human DLBCL cell lysates. A low exposure (l.e.) and high exposure (h.e.) are shown. A representative blot from two independent experiments is shown.
- (e)** Immunoblot analysis of whole cell lysates from OCI-LY10 cells electroporated with indicated siRNAs and treated with cycloheximide (CHX). Quantification and statistical analysis is shown in Fig. S2d.
- (f)** *KLHL6*^{+/+} and *KLHL6*^{-/-} U2932 cells(clone-derived) were processed as in (e). A low exposure (l.e.) and high exposure (h.e.) are shown. Quantification and statistical analysis is shown in Fig. S2d.
- (g)** Schematic representation of KLHL6 protein displaying endogenous mutations in VAL and SUDHL10 (top panel). Bottom panel shows immunoblot analysis from immunoprecipitated FLAG-tagged KLHL6 wild-type (WT), KLHL6 mutants (L24R, A25E, N60T, and T72R), or empty vector (EV) in HEK293T cells.
- (h)** Immunoblot analysis of whole cell lysates from VAL and SUDHL10 cells electroporated with siRNA scramble (siCTRL) or targeting KLHL6 (siKLHL6).
- (i)** Analysis of level of KLHL6 mRNA by quantitative PCR(qPCR). The value for the PCR product from U2932 cells was set as 1. A representative graph from two independent experiments is shown.
- (j)** Immunoblot analysis of whole cell lysates from VAL and SUDHL10 cells stably expressing KLHL6 under a doxycycline (DOX) inducible promoter with a puryomycin cassette after 12h of DOX treatment.
- (k)** *In vitro* ubiquitylation reaction of immunopurified FLAG-KLHL6 and HA-Roquin2. Unprocessed original scan of immunoblots for (b,c,d,e,f,g,h,j,k) are shown in Supplementary Fig. 8, and source data for (i) can be found in Supplementary Table 6. Unless otherwise noted, immunoblots are representative of three independent experiments.

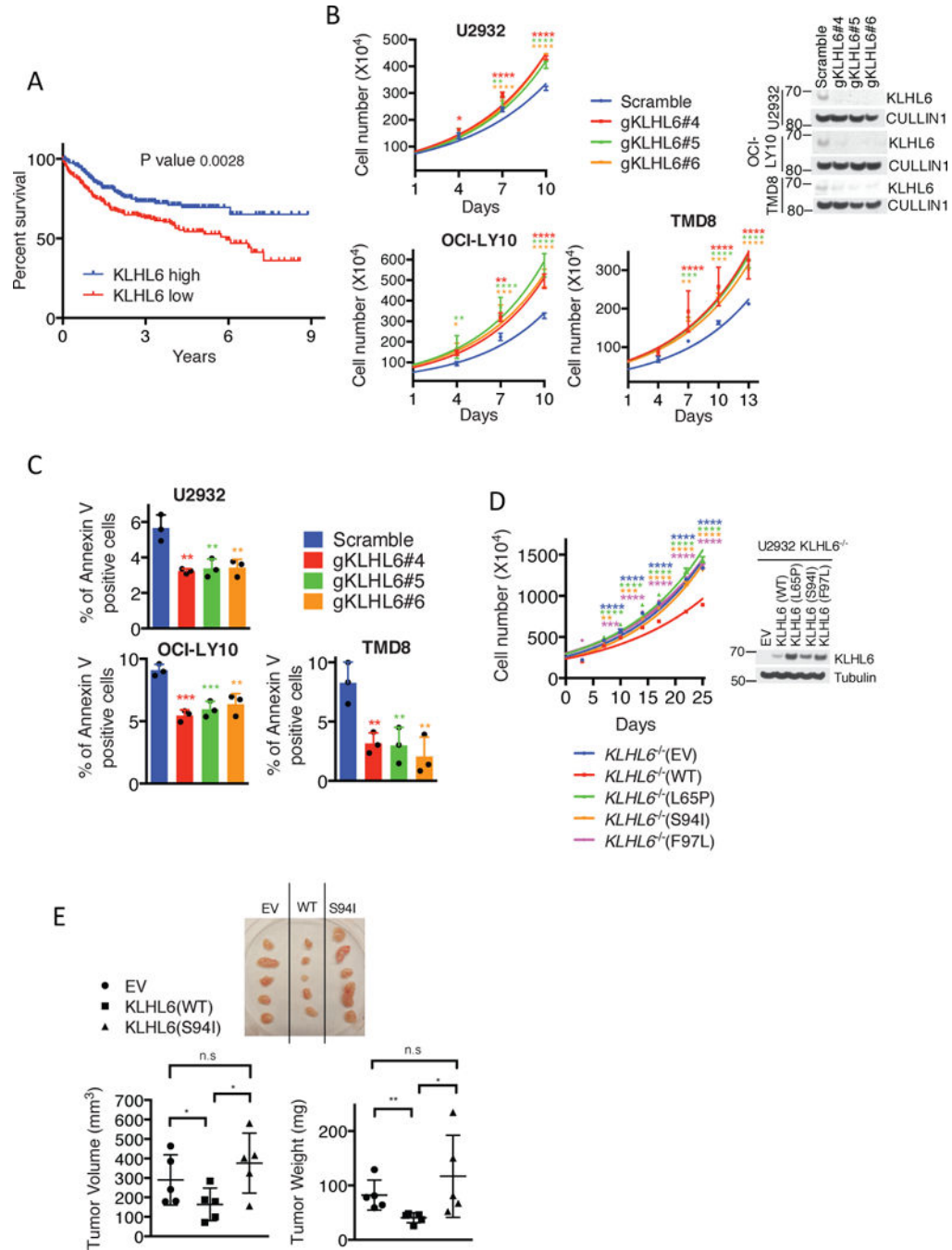


Figure 3. KLHL6 functions as a tumor suppressor in ABC-DLBCL by regulating its growth and survival

(a) Kaplan–Meier analysis based on gene expression data for ABC-DLBCL tumors (GSE10846, GSE34171 and GSE3131239-41) is shown ($n=367$ patients). Censored subjects are indicated on the Kaplan–Meier curve as tick mark. Statistical analysis was performed using the Log-rank (Mantel-Cox), two-sided test, 95% confidence interval.

(b) Cell counts of U2932-, OCI-LY10- and TMD8-Cas9 cells expressing the indicated gRNAs and carrying a puromycin cassette (mean \pm s.d., $n=3$ independent experiments, two-

way ANOVA, *P value 0.05; **P value 0.01; *** P value 0.001; ****P value 0.0001) (left panel). Cells were grown in media containing 1 μ g/ml (U2932- and OCI-LY10) or 4 μ g/ml (TMD8) of F(ab')₂-IgM. Right panel shows immunoblot analysis of whole cell lysates.

(c) Apoptosis analysis of U2932-, OCI-LY10-, and TMD8-Cas9 cells expressing the indicated gRNAs and carrying a GFP marker. Cells were grown as in (b). Apoptosis was quantified on GFP⁺ and Annexin V⁺ cells (mean \pm s.d., n=3 independent experiments, one-way ANOVA, **P value 0.01; *** P value 0.001).

(d) Left panel shows cell counts of GFP-sorted U2932 *KLHL6*^{-/-} (clone-derived) cells expressing empty vector (EV), KLHL6(WT) or BTB-mutants (L65P, S94I and F97L) and carrying a GFP marker (mean \pm s.d., n=3 independent experiments, two-way ANOVA, **P value 0.01; *** P value 0.001; ****P value 0.0001). Right panel shows the immunoblot analysis of whole cell lysates.

(e) Xenograft experiments with GFP-sorted U2932 *KLHL6*^{-/-} cells expressing an empty vector (EV), KLHL6(WT) or KLHL6(S94I) and carrying a GFP marker. Top panel shows the tumors at the experimental endpoint. Tumor volume (mean \pm s.d., n=5 mice per group, one-way ANOVA, *P value 0.05; n.s, not significant) and tumor weight (mean \pm s.d., n=5 mice per group, one-tailed t-test, *P value 0.05; **P value 0.01; n.s, not significant) are shown in the bottom left and right, respectively.

Unprocessed original scan of immunoblots for (b,d) are shown in Supplementary Fig. 8, and statistical source data and exact P values for (a,b,c,d,e) can be found in Supplementary Table 6. Unless otherwise noted, immunoblots are representative of three independent experiments.

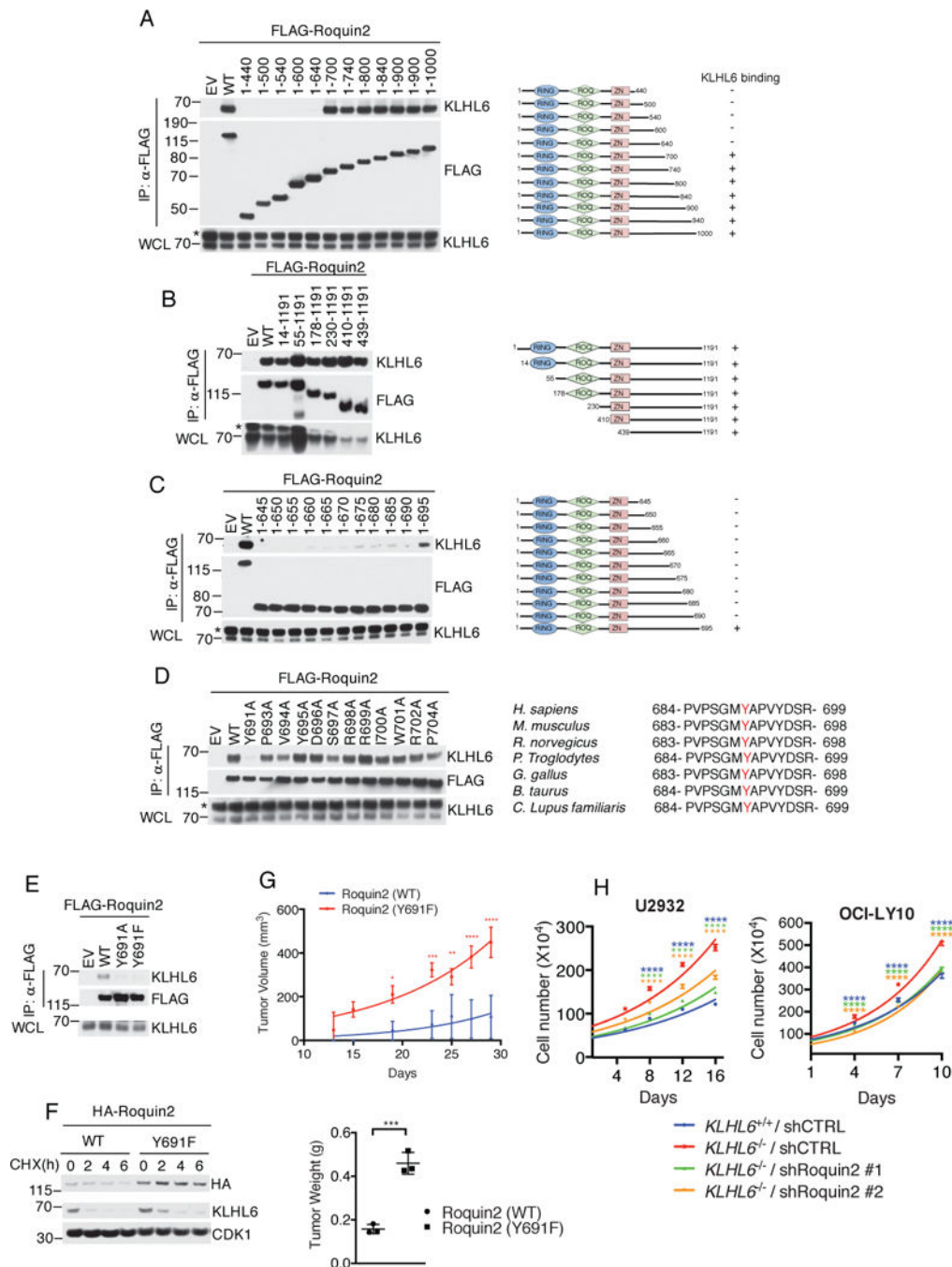


Figure 4. A non-degradable Roquin2 mutant phenocopies loss of KLHL6

(a) Left panel shows immunoblot analysis of immunoprecipitated FLAG-tagged Roquin2 wild type (WT) or mutants in HEK293T cells stably expressing KLHL6. EV, Empty vector. Right panel shows a schematic representation of Roquin2 mutants. Roquin2 mutants that interact (+) or do not interact (-) with KLHL6 are shown. A representative blot from two independent experiments is shown. Asterisk indicates non-specific bands. (b-d) Same as in (a).

(e) Immunoblot analysis of immunoprecipitated FLAG-tagged Roquin2 wild type (WT) or mutants, as indicated, in HEK293T cells stably expressing KLHL6. EV, Empty vector.

(f) Immunoblot analysis of whole cell lysates from a DLBCL cell line, BJAB, retrovirally transduced with cDNAs encoding Roquin2(WT) or Roquin2(Y691F) carrying a puromycin cassette. Cells were treated with cycloheximide (CHX) for the indicated times.

Quantification and statistical analysis is shown in Fig. S4e.

(g) Top panel shows tumor volume from subcutaneously injected NSG mice with U2932 cells stably expressing retroviruses encoding HA-Roquin2(WT) or HA-Roquin2(Y691F) carrying a puromycin cassette (mean±s.d., n=3 mice per group, two-way ANOVA, *P value 0.05; **P value 0.01; *** P value 0.001; ****P value 0.0001). Bottom panel shows tumor weight (mean±s.d., n=3 mice per group, two-tailed t-test, *** P value 0.001).

(h) Cell counts of GFP-sorted U2932 (left panel) or OCI-LY10 (right panel) *KLHL6*^{+/+} and *KLHL6*^{-/-} (clone-derived) cells infected with scramble shRNA(shCTRL) or shRNA targeting Roquin2 (ShRoquin2#1 or #2) carrying a GFP marker. GFP⁺ cells were grown in media containing 1µg/ml of F(ab')₂-IgM. (mean±s.d., n=3 independent experiments, two-way ANOVA, ****P value 0.0001).

Unprocessed original scan of immunoblots for (a,b,c,d,e,f) are shown in Supplementary Fig. 8, and statistical source data and exact P values for (g,h) can be found in Supplementary Table 6. Unless otherwise noted, immunoblots are representative of three independent experiments.

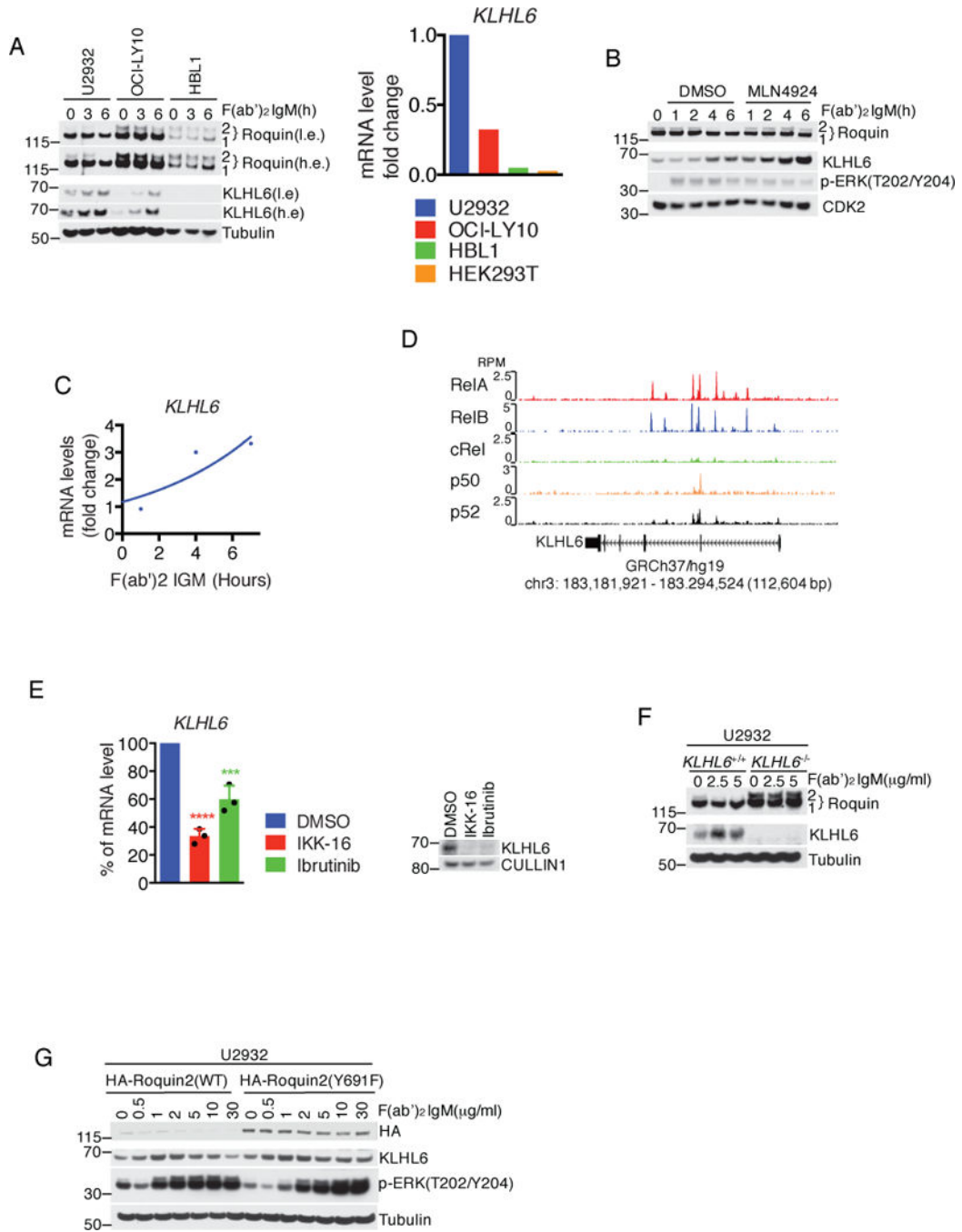


Figure 5. KLHL6 is a BCR/NF- κ B target gene that links Roquin2 degradation to BCR signaling (a) Immunoblot analysis of whole cell lysates from OCI-LY10, U2932, and HBL1 cells stimulated with 10 μ g/ml F(ab')₂-IgM for 3 and 6 hours (left panel). A low exposure (I.e.) and high exposure (h.e.) are shown. Right panel shows level of *KLHL6* mRNA analyzed by qPCR. The value for the PCR product from U2932 was set as 1. A representative graph from two independent experiments is shown.

- (b)** Immunoblot analysis of whole cell lysates from U2932 cells treated with 10 µg/ml of F(ab')₂-IgM for the indicated times. Where indicated, cells were pre-treated with 5µM MLN4924 for 1 hour.
- (c)** Analysis of level of *KLHL6* mRNA by qPCR in U2932 cells treated with 10 µg/ml of F(ab')₂-IgM for the indicated times. A representative graph from two independent experiments is shown. The value for PCR product without treatment was set as 1.
- (d)** Visualization of ChIP-seq peaks using the University of California Santa Cruz (UCSD) Genome browser (GEO Series accession GSE55105). RPM, reads per million mapped.
- (e)** Same as in (c) except that U2932 cells were treated with DMSO, 10µM of IKK inhibitor (IKK-16) or 5µM of BTK inhibitor (Ibrutinib) for 6 hours. The value for PCR product present without treatment (DMSO) was set as 100% (mean±s.d., n=3 independent experiments, one-way ANOVA, *** P value 0.001; ****P value 0.0001). The right panel shows immunoblot analysis of whole cell lysates for the indicated proteins.
- (f)** Immunoblot analysis of whole cell lysates from U2932 *KLHL6*^{+/+} and *KLHL6*^{-/-} (clone-derived) cells treated with increasing concentrations of F(ab')₂-IgM for 6 hours.
- (g)** Immunoblot analysis of whole cell lysates from U2932 cells stably expressing HA-Roquin2(WT) or HA-Roquin2(Y691F) treated with F(ab')₂-IgM for 6 hours.
- Unprocessed original scan of immunoblots for (a,b,e,f,g) are shown in Supplementary Fig. 8, and source data for (a,c) and statistical source data and exact P values for (e) can be found in Supplementary Table 6. Unless otherwise noted, immunoblots are representative of three independent experiments.

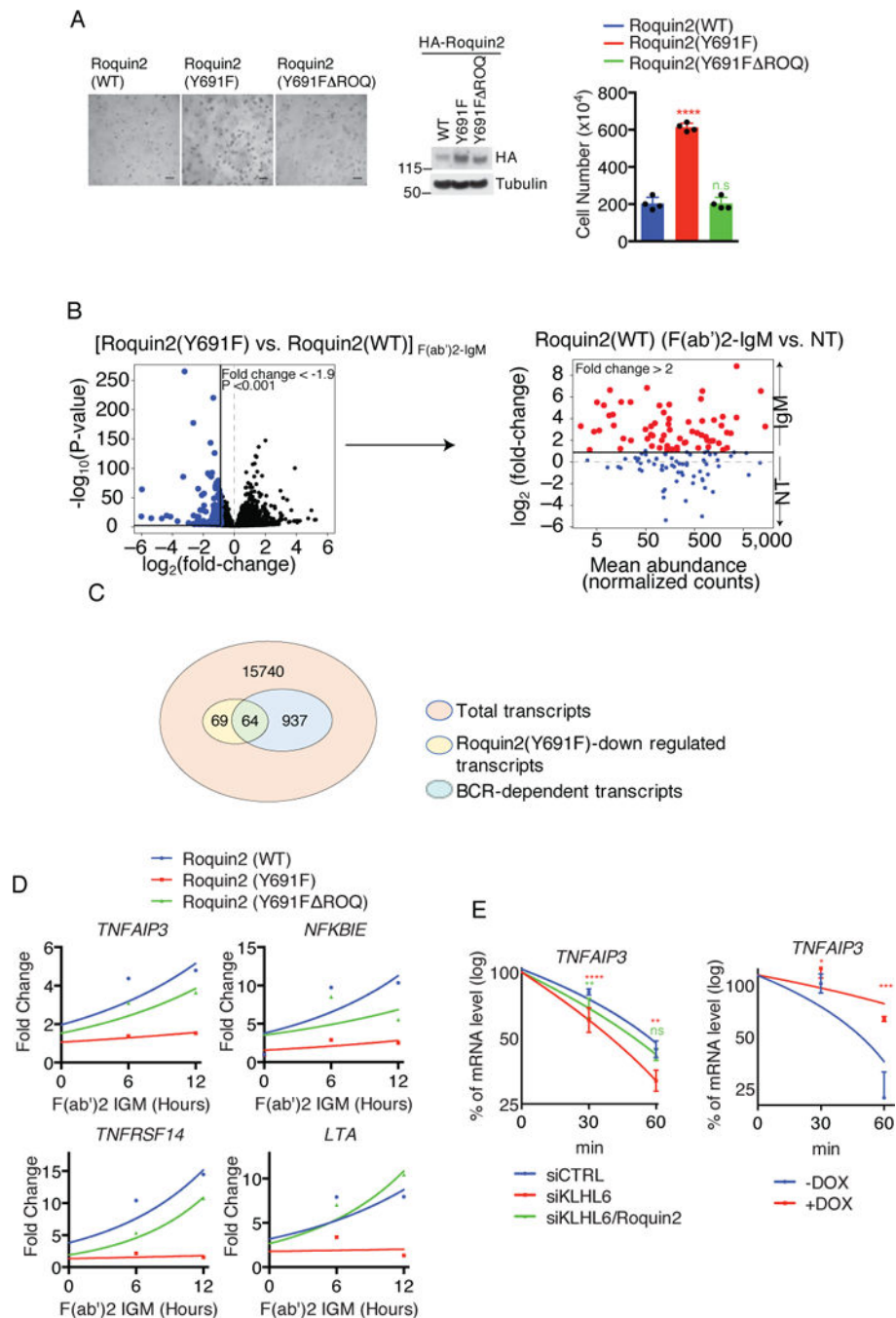


Figure 6. Stabilization of Roquin2 down-regulates BCR responsive genes

(a) Representative image of U2932 cells expressing HA-Roquin2(WT), HA-Roquin2(Y691F) or HA-Roquin2(Y691F ROQ) with puromycin cassette plated into a matrigel (Left panel). Middle panel shows immunoblot analysis of whole cell lysates and right panel shows cell counts from the matrigel (mean \pm s.d., n=4 independent experiments, one-way ANOVA, ****P value 0.0001, n.s, not significant). Scale bar 150 μ m.

(b) Volcano plot (left panel) showing down-regulated mRNAs (blue) in U2932 cells expressing Roquin2(Y691F) vs Roquin2(WT) upon 12 hours treatment with 10 μ g/ml of

F(ab')₂-IgM [$\log_2(\text{fold-change}) < -0.9$]. Down-regulated mRNAs were further plotted in an MA (log ratio, mean average)-plot (right panel). The mRNAs up-regulated upon treatment with F(ab')₂-IgM in cells expressing Roquin2(WT) [$\log_2(\text{fold-change}) > 1$] are shown in red. (n=3 independent experiments, DESeq2, P value < 0.001). NT, non treated.

(c) Venn diagram showing the overlap between genes down-regulated by expression of Roquin2(Y691F) and BCR responsive genes.

(d) qPCR analysis of the indicated mRNAs in U2932 cells expressing HA-Roquin2(WT, Y691F or Y691F ROQ) treated with 10 $\mu\text{g/ml}$ of F(ab')₂-IgM for indicated times. Value for PCR product present at time 0 hour was set as 1 for each condition. A representative graph from two independent experiments is shown.

(e) qPCR analysis of *TNFAIP3* mRNA in U2932 cells electroporated with indicated siRNAs (left panel) and treated with actinomycinD for the indicated times. The value for PCR product present at time 0 hour was arbitrarily set as 100% (mean \pm s.d., n=3 independent experiments, two-way ANOVA, **P value 0.01, ****P value 0.0001, n.s, not significant). Same analysis was performed in VAL cells expressing *KLHL6* under a DOX-inducible promoter (Right panel). Cells were pre-treated with DOX for 12 hours and actinomycinD for the indicated times (mean \pm s.d., n=3 independent experiments, two-way ANOVA, *P value 0.05; *** P value 0.001).

Unprocessed original scan of immunoblots for (a) are shown in Supplementary Fig. 8, and source data for (d) and statistical source data and exact P values for (a,e) and (b) can be found in Supplementary Table 6 and 3, respectively. Unless otherwise noted, immunoblots are representative of three independent experiments.

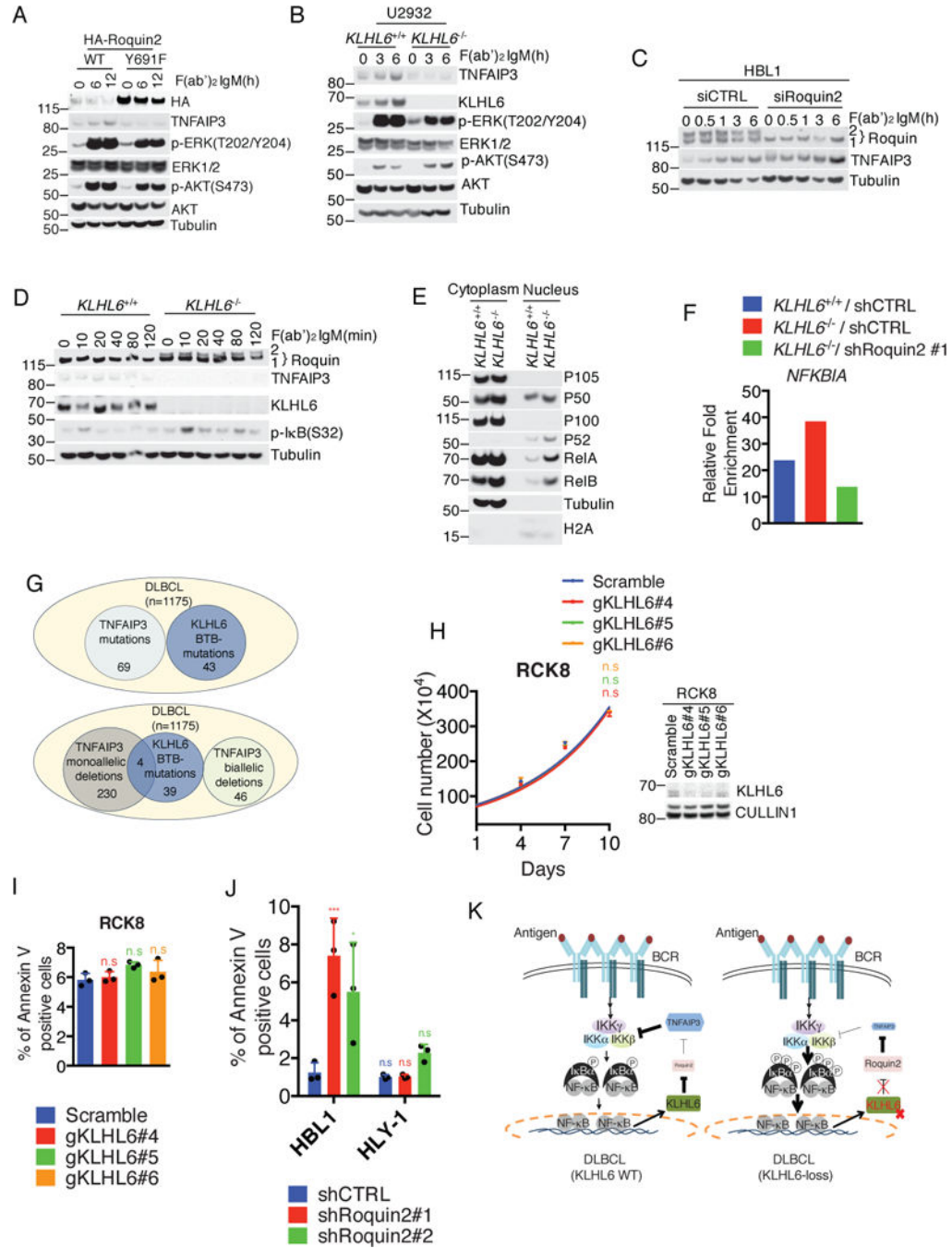


Figure 7. KLHL6-Roquin2 axis controls NF-κB activation

(a) Immunoblot analysis of whole cell lysates from U2932 cells expressing HA-Roquin2(WT) or HA-Roquin2(Y691F) treated with 10μg/ml of F(ab')₂-IgM for the indicated times.

(b) Immunoblot analysis of whole cell lysates from U2932 *KLHL6*^{+/+} or *KLHL6*^{-/-} cells (clone-derived) treated with 10μg/ml of F(ab')₂-IgM for the indicated times.

(c) Immunoblot analysis of whole cell lysates from HBL1 cells electroporated with indicated siRNAs and treated as in (a) for the indicated times.

- (d)** Immunoblot analysis of whole cell lysates from U2932 *KLHL6*^{+/+} or *KLHL6*^{-/-} cells (clone-derived) treated with 10µg/ml of F(ab')₂-IgM for the indicated times.
- (e)** Immunoblot analysis of fractionated U2932 *KLHL6*^{+/+} or *KLHL6*^{-/-} (clone-derived) cells.
- (f)** RelA ChIP-qPCR for the *NFBK1A* promoter in U2932 *KLHL6*^{+/+}, *KLHL6*^{-/-} or *KLHL6*^{-/-} cells infected with indicated shRNAs. Data are displayed as fold enrichment relative to IgG control. A representative graph from two independent experiments is shown.
- (g)** Overlap of BTB-associated mutations of *KLHL6* with *TNFAIP3* alterations in DLBCLs. Top panel shows tumors sequenced at UNMC⁶ and DCI⁷ (n=1175) with deleterious mutations of *KLHL6* in the BTB-domain and *TNFAIP3* mutations. In the bottom panel, the *TNFAIP3* subset is shown as biallelic and monoallelic deletions.
- (h)** Cell counts of GFP-sorted RCK8 cells expressing Cas9, the indicated gRNAs and a GFP marker. Cells were grown in media containing 1µg/ml of F(ab')₂-IgM (mean±s.d., n=3 independent experiments, two-way ANOVA, n.s, not significant). Right panel shows immunoblot analysis of whole cell lysates.
- (i)** Apoptosis analysis of cells from (h) is shown (mean±s.d., n=3 independent experiments, one-way ANOVA, n.s, not significant).
- (j)** The percentage of GFP⁺ and AnnexinV⁺ HBL1 and HLY-1 cells expressing the indicated shRNAs is shown (mean±s.d., n=3 independent experiments, one-way ANOVA, *P value 0.05; *** P value 0.001, n.s, not significant).
- (k)** Model of *KLHL6*-Roquin2 axis in ABC-DLBCL.
- Unprocessed original scan of immunoblots for (a,b,c,d,e,h) are shown in Supplementary Fig. 8, and source data for (f) and statistical source data for (h,i,j) and exact P values for (j) can be found in Supplementary Table 6. Unless otherwise noted, immunoblots are representative of three independent experiments.